

# **Scalability of the LEU-Modified Cintichem Process: 3-MeV Van de Graaff and 35-MeV Electron Linear Accelerator Studies**

---

**Nuclear Engineering Division**

### **About Argonne National Laboratory**

Argonne is a U.S. Department of Energy laboratory managed by UChicago Argonne, LLC under contract DE-AC02-06CH11357. The Laboratory's main facility is outside Chicago, at 9700 South Cass Avenue, Argonne, Illinois 60439. For information about Argonne and its pioneering science and technology programs, see [www.anl.gov](http://www.anl.gov).

### **DOCUMENT AVAILABILITY**

**Online Access:** U.S. Department of Energy (DOE) reports produced after 1991 and a growing number of pre-1991 documents are available free via DOE's SciTech Connect (<http://www.osti.gov/scitech/>)

### **Reports not in digital format may be purchased by the public from the National Technical Information Service (NTIS):**

U.S. Department of Commerce  
National Technical Information Service  
5301 Shawnee Rd  
Alexandria, VA 22312  
**[www.ntis.gov](http://www.ntis.gov)**  
Phone: (800) 553-NTIS (6847) or (703)  
605-6000 Fax: (703) 605-6900  
Email: [orders@ntis.gov](mailto:orders@ntis.gov)

### **Reports not in digital format are available to DOE and DOE contractors from the Office of Scientific and Technical Information (OSTI):**

U.S. Department of Energy  
Office of Scientific and Technical Information  
P.O. Box 62  
Oak Ridge, TN 37831-0062  
**[www.osti.gov](http://www.osti.gov)**  
Phone: (865) 576-8401  
Fax: (865) 576-5728  
Email: [reports@osti.gov](mailto:reports@osti.gov)

### **Disclaimer**

This report was prepared as an account of work sponsored by an agency of the United States Government. Neither the United States Government nor any agency thereof, nor UChicago Argonne, LLC, nor any of their employees or officers, makes any warranty, express or implied, or assumes any legal liability or responsibility for the accuracy, completeness, or usefulness of any information, apparatus, product, or process disclosed, or represents that its use would not infringe privately owned rights. Reference herein to any specific commercial product, process, or service by trade name, trademark, manufacturer, or otherwise, does not necessarily constitute or imply its endorsement, recommendation, or favoring by the United States Government or any agency thereof. The views and opinions of document authors expressed herein do not necessarily state or reflect those of the United States Government or any agency thereof, Argonne National Laboratory, or UChicago Argonne, LLC.

# **Scalability of the LEU-Modified Cintichem Process: 3-MeV Van de Graaff and 35-MeV Electron Linear Accelerator Studies**

---

by

David A. Rotsch, Tom Brossard, Ethan Roussin, Kevin Quigley,  
Sergey Chemerisov, Roman Gromov, Charles Jonah, Lohman Hafenrichter,  
Peter Tkac, John Krebs, and George F. Vandegrift  
Nuclear Engineering Division, Argonne National Laboratory

October 2016



# CONTENTS

<b>ABSTRACT</b> .....	<b>1</b>
<b>1 INTRODUCTION</b> .....	<b>2</b>
<b>2 EXPERIMENTAL</b> .....	<b>4</b>
2.1 Van de Graaff Experiments .....	4
2.1.1 VDG Temperature Studies .....	4
2.1.2 Further Characterization of the VDG Beam .....	6
2.1.3 VDG Oxalic Acid Dosimetry .....	6
2.1.4 VDG <sup>99</sup> Mo-ABO Experiments.....	7
2.2 Linac Experiments .....	7
2.2.1 Argonne Electron Linac.....	7
2.2.2 Linac Beam Profiling.....	8
2.2.3 <sup>99</sup> Mo-ABO Linac Irradiation Rotation Rig.....	12
2.2.4 Linac Temperature Profiling.....	16
2.2.5 Linac Oxalic Acid Dosimetry .....	18
2.2.6 Linac <sup>99</sup> Mo-ABO Experiments .....	18
<b>3 RESULTS AND DISCUSSION</b> .....	<b>19</b>
3.1 VDG Experiments.....	19
3.1.1 VDG Oxalic Acid Dosimetry Verification .....	19
3.1.2 VDG Correction Factor .....	20
3.1.3 VDG <sup>99</sup> Mo-ABO Irradiations .....	21
3.2 Linac Experiments .....	25
3.2.1 Linac Oxalic Acid Dosimetry .....	25
3.2.2 Linac <sup>99</sup> Mo-ABO Experiments .....	27
<b>4 CONCLUSIONS</b> .....	<b>37</b>
<b>ACKNOWLEDGMENTS</b> .....	<b>37</b>
<b>REFERENCES</b> .....	<b>38</b>

## FIGURES

1	<sup>99</sup> Mo-ABO irradiation system at VDG. Beam line exit window can be seen on the left. The <sup>99</sup> Mo-ABO target holder is on the right.....	4
2	Three-pronged compressed air cooling system of <sup>99</sup> Mo-ABO irradiation system at the VDG. The sample is located within the center of the aluminum block.....	5

## FIGURES (Cont.)

3	Temperature profile of blank sample during irradiation with a 3 MeV, 50 $\mu$ A beam with new cooling system.....	6
4	Example beam energy spectrum for the linac experiments. ....	8
5	Beam profile from scanned Plexiglas. Vertical line is shadow of target holder arm; all dimensions are in inches. Horizontal cross section of beam spot profile, intensity vs. inches. ....	9
6	Beam profile from scanned Plexiglas. Vertical line is the shadow of the target holder arm; all dimensions are in inches. Horizontal cross section of beam spot profile, intensity vs. inches with overlay of irradiation vessel. Irradiation vessel depicts approximate beam profile over vessel, the horizontal dimension of the vessel is to scale, the vertical dimension is not to scale.....	10
7	Beam profile from scanned Plexiglas. Vertical cross section of beam spot profile, intensity vs. inches with overlay of irradiation vessel. Irradiation vessel depicts approximate beam profile over vessel, the vertical dimension of the vessel is to scale, the horizontal dimension is not to scale. ....	11
8	Rotation mechanisms used to provide rotation of the sample during irradiation. Initial experiments utilized a drive chain. Other system components are depicted in the photo. ....	12
9	Finalized designs utilized a drive shaft that only provided 180° oscillation to allow for cooling lines. ....	13
10	Depiction of rotation system and mounted irradiation vessel on mock beam line. ....	14
11	Quartz irradiation vessels used during linac Mo-ABO trials. The vessels were quartz with a quartz-fritted funnel, and a quartz jacket for water cooling.....	14
12	Glove box used as secondary containment of the acid wash injection and vacuum systems.....	15
13	Schematic drawing of linac experimental setup .....	16
14	Temperature profile of quartz vessel under dry and wet conditions.....	17
15	Oxalic acid dosimetry results at various beam currents.....	19

## FIGURES (Cont.)

16	Correlation of Van De Graaff beam current measured on the beam shutter window and the aperture. Measurements were taken with shutter fully closed and correlated to the aperture currents when the shutter was open. The sample receives dose while the shutter is open and receives no dose when the shutter is closed. ....	20
17	Molybdenum recovery after applying a calculated dose of radiation with the VDG ...	23
18	Mo-ABO recovery based on age of non-irradiated samples.....	24
19	Oxalic acid dosimetry curve obtained at 12 in. from the beam exit window. A 35 MeV beam with 0.5 kW of power at 5 Hz was used during these irradiations....	25
20	Extrapolation of oxalic acid dosimetry to >7,000 Mrad. Error bars represent $\pm 10\%$ error in dose. ....	26
21	Mo-ABO precipitated in a quartz irradiation vessel with quartz beads prior to irradiation, and Mo-ABO and quartz irradiation vessel with quartz beads after irradiation. Images are of the first version of the irradiation vessel. These vessels were initially used during full 360° rotation of the vessel. Jacketed vessels were used in the final version. ....	27
22	Jacketed quartz irradiation vessel with Mo-ABO precipitated on the frit. Cooling lines are shown in the image. Chilled water from a recirculating bath was introduced from the bottom and expelled from the top. A thin layer of Mo-ABO is almost invisible to the eye.....	28
23	Mo-ABO precipitated in quartz vessel prior to irradiation. An aluminum window was used during these irradiations. The beam was spread with magnets and collimated with a lead brick and water-cooled beam stop. Hose clamps were used during all irradiations, not shown here. ....	29
24	Alternative view of Mo-ABO precipitated in quartz vessel prior to irradiation. Water-cooled beam stops can be seen between the beam window and the irradiation vessel, as well as behind the irradiation vessel. Hose clamps were used during all irradiations, not shown here. ....	29
25	Mo-ABO precipitated in quartz vessel after irradiation. The quartz darkened from exposure to the electron beam. Hose clamps are observed for the water cooling lines. Condensation can be seen on the exterior of the vessel. The condensation was from atmospheric water and does not represent a breach of containment.....	30

## FIGURES (Cont.)

26	Discoloration of Mo-ABO solid (visible through the darkened quartz walls). The movement of the Mo-ABO solid from the frit was attributed to the introduction of the wash solution from the bottom of the vessel.....	30
27	Combined HNO <sub>3</sub> wash solutions post-irradiation. The coloration did not have a direct link to activity. ....	31
28	Distribution of Mo-99 percentages in the HNO <sub>3</sub> wash, NaOH product, and residual on the frit .....	33
29	Percent of Mo-99 recovered and lost in relation to Mo-99 equivalent dose.....	34

## TABLES

1	Dose rates attained with various beam currents used at 3 MeV VDG.....	20
2	Molybdenum-99 dose equivalents calculated with correction term to account for current variations during experiments .....	21
3	Recovery of Mo-99 activity in the HNO <sub>3</sub> wash, NaOH product solution, and residual left on the filter .....	22
4	Measured percentages of Mo-99 recovered in the HNO <sub>3</sub> wash, NaOH product solution, and residual left on the filter .....	22
5	Recoverable and loss of Mo-99 relative to Mo-99 dose equivalence .....	24
6	Table relating Mo-99 dose equivalence as determined from oxalic acid dosimetry to Mo-ABO with geometric variable included .....	26
7	Distribution of Mo-99 activity in the HNO <sub>3</sub> wash, NaOH product, and residual on the frit.....	32
8	Distribution of Mo-99 percentages in the HNO <sub>3</sub> wash, NaOH product, and residual on the frit .....	32
9	Percent of Mo-99 recovered and lost from Mo-ABO linac experiments.....	33
10	Data used to determine the change in temperature for various activities of Mo-99.....	36

**TABLES (Cont.)**

11    Temperature increases of various activities of Mo-99 over several time periods  
      assuming complete deposition of the maximum beta emission in an adiabatic  
      system ..... 36



**SCALABILITY OF THE LEU-MODIFIED CINTICHEM PROCESS:  
3-MEV VAN DE GRAAFF AND 35-MEV ELECTRON LINEAR  
ACCELERATOR STUDIES**

**ABSTRACT**

Molybdenum-99, the mother of Tc-99m, can be produced from fission of U-235 in nuclear reactors and purified from fission products by the Cintichem process, later modified for low-enriched uranium (LEU) targets. The key step in this process is the precipitation of Mo with  $\alpha$ -benzoin oxime (ABO). The stability of this complex to radiation has been examined. Molybdenum-ABO was irradiated with 3 MeV electrons produced by a Van de Graaff generator and 35 MeV electrons produced by a 50 MeV/25 kW electron linear accelerator. Dose equivalents of 1.7–31.2 kCi of Mo-99 were administered to freshly prepared Mo-ABO. Irradiated samples of Mo-ABO were processed according to the LEU Modified-Cintichem process. The Van de Graaff data indicated good radiation stability of the Mo-ABO complex up to ~15 kCi dose equivalents of Mo-99 and nearly complete destruction at doses >24 kCi Mo-99. The linear accelerator data indicate that even at 6.2 kCi of Mo-99 equivalence of dose, the sample lost ~20% of Mo-99. The 20% loss of Mo-99 at this low dose may be attributed to thermal decomposition of the product from the heat deposited in the sample during irradiation.

## 1 INTRODUCTION

Technetium-99m is a widely used radioisotope for single-photon emission computed tomography (SPECT) imaging because of its ideal characteristics, such as a sufficiently short half-life (6 hours) and single gamma emission (140 keV). SPECT utilizes gamma emissions from select radioisotopes, such as  $^{99m}\text{Tc}$  (140 keV), to collect multiple 2D images that can later be combined into 3D images that map the interior of a patient. Information such as this provides insight on diseases that will help doctors cure certain ailments.

There is currently no US domestic supply of  $^{99m}\text{Tc}$  or its parent  $^{99}\text{Mo}$ . Argonne National Laboratory with the National Nuclear Security Administration's (NNSA) Office of Material Management and Minimization ( $M^3$ ), in partnership with SHINE Medical Technologies, is developing technologies for the domestic production of Mo-99 for nuclear medicine while minimizing the civilian use of highly enriched uranium-235 (HEU). SHINE is planning to produce Mo-99 by fission of low enriched uranium-235 (LEU) in a subcritical aqueous solution using accelerator-based neutron generation [1].

The Cintichem process has been modified for the purification of Mo-99 from LEU targets. This LEU-Modified Cintichem process (LMC) has been chosen by SHINE to purify its subcritical-produced Mo-99 [2,3]. The LMC rarely processed more than 1,000 Ci of Mo-99 in a single batch. SHINE plans to produce and purify up to 6000 Ci in a single batch. In this process, Mo(VI) is precipitated by  $\alpha$ -benzoin oxime (ABO), a standard analytical method for molybdenum quantification [4,5, 6–11]. ABO is the key reagent of the Cintichem and LMC processes, allowing for selective precipitation of molybdenum from acidic solutions ( $\sim 1\text{ M HNO}_3$ ), where molybdenum is present as the molybdenyl cation ( $\text{MoO}_2^{2+}$ ).

A concern is that ABO will break down under the high dose conditions provided by thousands of Ci of Mo-99, and the recovery of Mo-99 will decrease. Expected doses received by the Mo-ABO complex from Mo-99 emissions were determined through computational studies. Simulations with MCNPX [12] were conducted under several conditions and provided a link between Mo-99 activity and the dose received by the Mo-ABO complex. For a more conservative scenario, the Mo-ABO precipitate was present as a monolayer during simulations; it was determined that a Mo-ABO precipitate containing 1 kCi of Mo-99 receives a dose of 148.3 Mrad [12].

Experimentally administered doses were determined by the use of oxalic acid dosimetry. Oxalic acid samples of similar geometry as the Mo-ABO complex were irradiated and analyzed to experimentally determine the dose received by the sample from irradiation experiments using Argonne's 3 MeV Van de Graaff (VDG) generator. It had been shown that oxalic acid can be used as a dosimeter in aqueous solution [13]. Other aqueous chemical dosimeters exist but oxalic acid holds advantages over them, such as 1) higher dose limits, 2) no activation of the dosimeter, and 3) insensitivity to impurities and light. The dose is determined by comparing the concentration of acid prior to and after irradiation as the acid decomposes with irradiation [13].

Previous experiments utilizing the Argonne 3 MeV VDG gave an indication that the Mo-ABO precipitate would not begin to lose Mo-99 until over 41,000 Ci of Mo-99 when dry or 10,000 Ci when in contact with nitric acid was processed [14]. Samples were placed directly next to the VDG beam exit window and irradiated for various time lengths at set beam parameters. The narrow beam introduced beam “wandering,” and thus errors in perceived doses; these experiments have been repeated using a wider beam. A wider beam allowed for a more uniform irradiation zone, and thus a more uniform dose, even if beam “wandering” occurs.

A series of experiments utilizing a wider beam were performed and previously reported [15,16]. Experimental data utilizing a spread beam demonstrated good radiation stability of the Mo-ABO complex up to ~12.5 kCi dose equivalents of Mo-99 when covered with HNO<sub>3</sub>. At higher doses, the decomposition of the Mo-ABO complex led to the formation of Mo species that were soluble in HNO<sub>3</sub> (10–20% Mo-99 loss) and caused a noticeable decrease in Mo recovery. The stability of the complex under dry conditions was not investigated.

The “breaking point” of the Mo-ABO complex was not achieved during these experiments. Therefore, irradiations of the Mo-ABO precipitate at higher doses were investigated and reported here. Irradiations performed in the previous work utilized the VDG, operated with beam currents of 30 μA. These irradiations required >10 hours in order to obtain doses >15 kCi dose equivalents of Mo-99. By increasing the beam current to 50 μA, higher dose rates can be achieved, minimizing the required irradiation time. The previous system was modified to allow for better cooling at higher beam currents, and irradiations ensued [16].

The VDG irradiations were performed on scaled-down samples of Mo-ABO covered with HNO<sub>3</sub>, which does not represent actual processing. During the LMC process, the Mo-ABO complex is washed with three 20 mL and five 10 mL aliquots of HNO<sub>3</sub>. Therefore, to better represent experimental conditions, a remotely operated irradiation system capable of washing the Mo-ABO complex during irradiation was developed and irradiated under high-dose conditions provided by Argonne’s electron linac [16]. The results of these experiments are described herein.

## 2 EXPERIMENTAL

### 2.1 VAN DE GRAAFF EXPERIMENTS

Irradiations were performed with a well-characterized experimental system [15,16]. The beam striking the target was characterized by use of a Faraday cup placed 15 in. away from the beam exit window. The cup was then moved from center in half-inch increments to obtain a profile. The temperature of the system during the characterization process was monitored by immersing a thermocouple in a suspension of Mo-ABO in HNO<sub>3</sub> (0.1 M). A 3 MeV beam with current of 50  $\mu$ A was used during these trials. It was found that the solution required cooling with chilled compressed gas flow over the exterior of the irradiation vessel (Figure 1) [15,16].



**FIGURE 1** <sup>99</sup>Mo-ABO irradiation system at VDG. Beam line exit window can be seen on the left. The <sup>99</sup>Mo-ABO target holder is on the right.

#### 2.1.1 VDG Temperature Studies

The temperature of a blank sample was monitored with a thermocouple to obtain a temperature profile during irradiation. Molybdenum was precipitated with ABO, isolated, covered with HNO<sub>3</sub>, and used to obtain a temperature profile that mimicked the sample during experimental irradiation. A thermocouple was immersed in the Mo-ABO sample in HNO<sub>3</sub> (0.1 M, 200  $\mu$ L). To prevent boiling of the solution, the sample needed to be cooled. A copper coil was attached to the compressed air lines and submerged in a salted ice bath prior to passing

the stream of air through the coil and over the sample. The compressed air was forced through the three-pronged cooling system shown in Figure 2.



**FIGURE 2** Three-pronged compressed air cooling system of  $^{99}\text{Mo}$ -ABO irradiation system at the VDG. The sample is located within the center of the aluminum block.

The temperature of the sample during irradiation was found to stabilize after 7–10 minutes of irradiation with a 3 MeV, 50  $\mu\text{A}$  beam. Cooling was applied by forced air fed through a salted ice bath on three sides of the vessel. With cooling in this manner, the temperature reached  $\sim 24^\circ\text{C}$  after  $\sim 3$  minutes and leveled to  $\sim 22^\circ\text{C}$  after 7–10 minutes (Figure 3). The temperature did not change significantly over time. For longer irradiations, the salted ice bath was replaced as necessary.

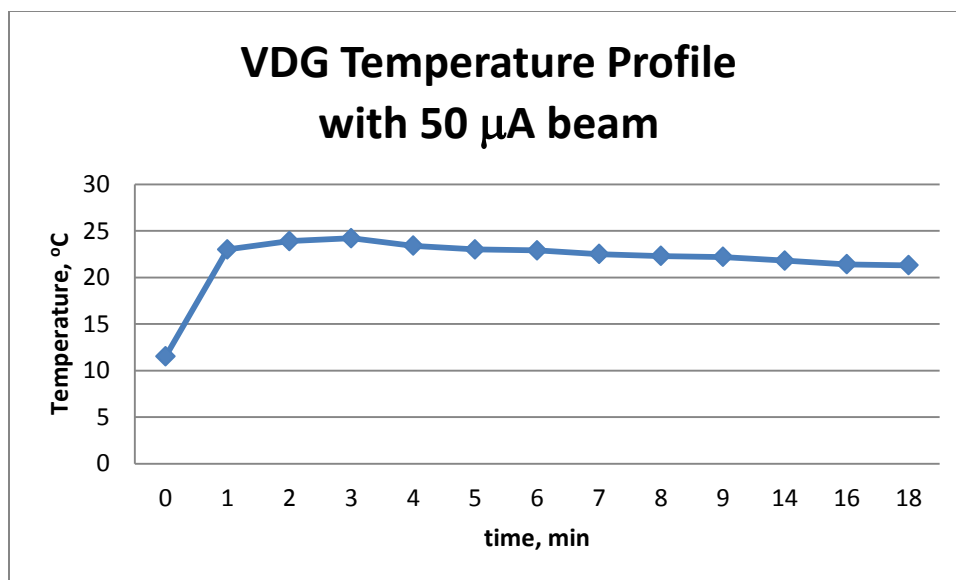


**FIGURE 3** Temperature profile of blank sample during irradiation with a 3 MeV, 50 μA beam with new cooling system

### 2.1.2 Further Characterization of the VDG Beam

The VDG beam current was determined by measuring the current on an aperture. The aperture did not represent the actual beam current, as it only “scrapes” part of the beam. The full current can be measured by the shutter window; however, with the shutter window closed, the target cannot be irradiated. Therefore, a relationship between the current measured on the aperture and that measured on the shutter window was required. This relationship was determined by measuring the current on a closed shutter window and comparing that to the current measured on the aperture with the shutter open.

### 2.1.3 VDG Oxalic Acid Dosimetry

Doses were determined by oxalic acid dosimetry. A solution of oxalic acid (~0.6 M, 1 mL) was irradiated with a 3 MeV, 50 μA beam at 15 in. from the window for various time periods and cooled with a constant stream of compressed air (chilled by a salted ice bath). The clear glass test tube browned over time. Irradiated solutions of oxalic acid (0.9 mL) were titrated with standardized NaOH to determine the final concentration of oxalic acid. The results were plotted to obtain a linear dose curve. It is important to realize that the dose is extremely dependent on the position of the sample. Even slight variations in the sample’s position will dramatically alter the dose received. Therefore, dose calibrations must be obtained with the rig in place prior to experimental work.

### 2.1.4 VDG <sup>99</sup>Mo-ABO Experiments

Molybdenum carrier solution (10 mg-Mo/mL) was prepared by dissolving MoO<sub>3</sub> in NaOH (1 M) and neutralizing it with HNO<sub>3</sub> (8 M). Prior to precipitation with ABO, the Mo carrier solution was spiked with a known amount of Mo-99. ABO (2%) was prepared by dissolution of ABO in hot NaOH (0.4 M). Mo-carrier (11.0 μL) spiked with Mo-99 was diluted with HNO<sub>3</sub> (~1.43 M, ~1.47 mL) and oxidized with KMnO<sub>4</sub> (2.5% KMnO<sub>4</sub>, 68 μL). The resultant solution was mixed and then precipitated with the ABO stock solution (453 mL). The mixture was centrifuged and the supernatant was removed. Mo-ABO solid was covered with HNO<sub>3</sub> (0.1 M, 200 μL) and irradiated in a glass vial. After irradiation, the samples were filtered using a 0.22 μm PVDF membrane filter (Millipore). The vessel and filter were washed with HNO<sub>3</sub> (0.1 M, 2.0 mL). The wash was kept for gamma counting. The Mo-ABO precipitate was dissolved from the filter using a hot NaOH/H<sub>2</sub>O<sub>2</sub> solution (0.4 M NaOH, 1% H<sub>2</sub>O<sub>2</sub>, 1.5 mL). To ensure complete dissolution of the ABO-Mo precipitate, the filter was washed with an additional 1.0 mL of NaOH/H<sub>2</sub>O<sub>2</sub> (0.2 M NaOH, 1% H<sub>2</sub>O<sub>2</sub>). Another NaOH wash (0.2 M, 0.5 mL) was used to rinse any remaining residue left on the filter. All NaOH fractions were collected, combined, and kept for gamma counting. A high-purity germanium (HPGe) gamma detector was used to determine the amount of Mo-99 (739.4 keV emission) in the HNO<sub>3</sub> wash, NaOH product, and any remaining on the filter.

It should be noted that under these scaled-down conditions it was difficult to achieve quantitative dissolution of the Mo-ABO complex, and some Mo was left on the filter. In the LMC process, the Mo-ABO complex is dissolved using a NaOH/H<sub>2</sub>O<sub>2</sub> mixture, heated (via heat gun), and shaken in the presence of glass beads to achieve quantitative dissolution. Moreover, the dissolved Mo in the NaOH solution is removed from the glass filter using a vacuum, which leads to a very high Mo recovery. These conditions are difficult to replicate in small-scale experiments.

## 2.2 LINAC EXPERIMENTS

### 2.2.1 Argonne Electron Linac

Argonne's low-energy and high-power electron linac was used to provide a higher dose rate for the experiments than that achievable with the VDG. This machine operates with a repetition rate up to 240 Hz with ultimate beam power up to 110 W per pulse. The effective beam energy is in the range from 20 to 45 MeV. The highest beam energy is about 50 MeV. A DC thermal gun produces an electron beam with current up to 2.0 A and length about 5.5 μS. The RF power is provided by two THALES TV2022A klystrons. After acceleration, the beam travels through the transport channel to the experimental hall and is delivered to the target face. Steering coils and quad magnets keep the beam in proper shape and position [17].

The Mo-ABO irradiations were performed with beam energy of  $35.0 \pm 0.5$  MeV (Figure 4). The injector pulse current was 0.7 A, and the accelerated pulse current was about 0.6 A, which corresponds to 86% of pulse bunching efficiency. The average beam power for irradiation was chosen to be 0.5 kW, which was restricted by the target cooling system capacity. The average beam current was about 15  $\mu$ A at the repetition rate of 5 Hz.

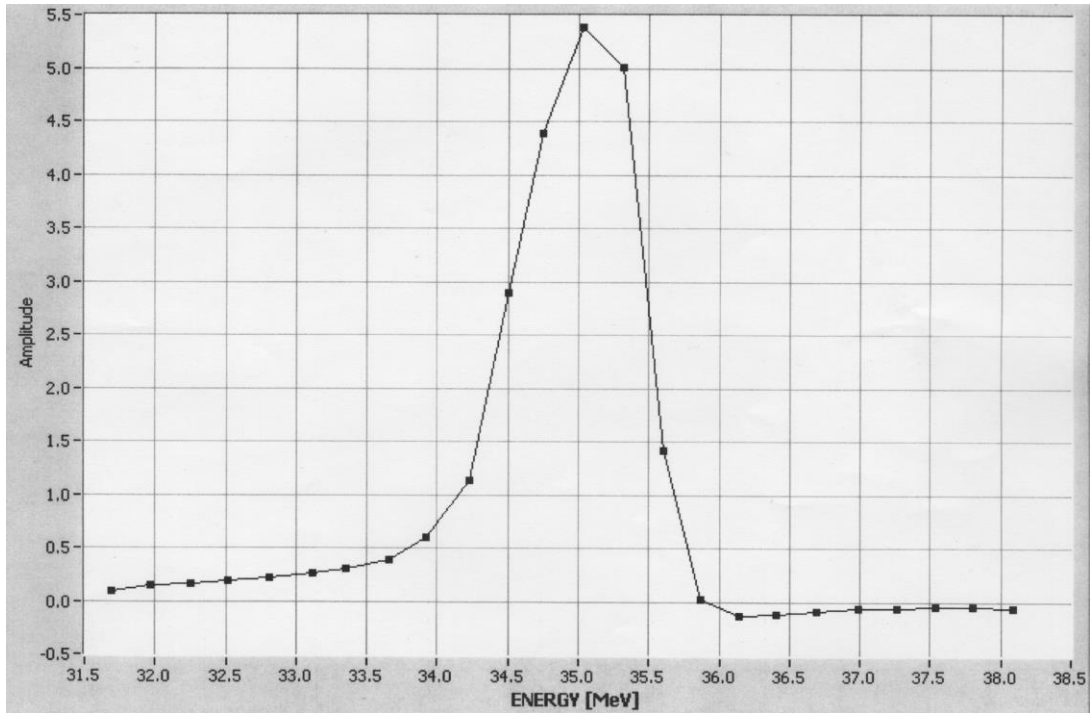


**FIGURE 4** Example beam energy spectrum for the linac experiments

## 2.2.2 Linac Beam Profiling

The electron beam was defocused in the horizontal plane and focused in the vertical. A water-cooled collimator was installed between the target and beam line output window in order to decrease undesired irradiation of the surrounding area.

The profile of the beam was checked with Plexiglas (Perspex) slides. Plexiglas has been used and studied as a dosimeter for more than 50 years [18–20]. The exposed Plexiglas was scanned in transmission (film mode) using a conventional flat-bed scanner (Epson Expression 10000 XL) in a 48-bit RGB mode. The blue channel was isolated, and the optical density was calculated. The 100% light was measured at a blank spot on the slide, and the zero light was determined where an opaque object was placed on the slide.

Understanding the beam profile was very important for these experiments. A pencil beam would provide too high of a power density and not evenly distribute the dose. The beam was defocused to irradiate as much of the volume of the target material as possible. The beam was

flattened in the horizontal direction for these irradiations, as seen in Figures 5–7. To achieve this, the last quadrupole’s doublet was used like a beam spot shape forming system. The beam spot was found to be approximately 0.5 in.  $\times$  1.0 in. laterally and longitudinally. The peak intensity of the beam was found to be within an ellipsoid centralized within the full beam spot. The irradiation vessel was 1.75 in. across where the Mo-ABO target material was held (Figure 6). This length was deemed acceptable as the vessel rotation helped to evenly distribute the beam across the target in the horizontal.

An approximation of the dose over the oxalic acid dosimeter compared to the Mo-ABO complex was required as the height of the Mo-ABO sample was small relative to the height of the electron beam, and the height of the oxalate solution was not relative to the height of the electron beam. The width of the beam at half height is approximately 0.85 cm. The average of the beam over the height of the sample compared to the average at the peak is approximately 0.7, so the relative dose into the ABO is expected to be about 50% higher than that of the dosimeter solution. Note that this estimate is only approximate (Figures 6 and 7). This correction was taken into account during the Mo-ABO trials, where 50% dose was attributed to the Mo-ABO compared to that which was expected from the oxalic acid trials.

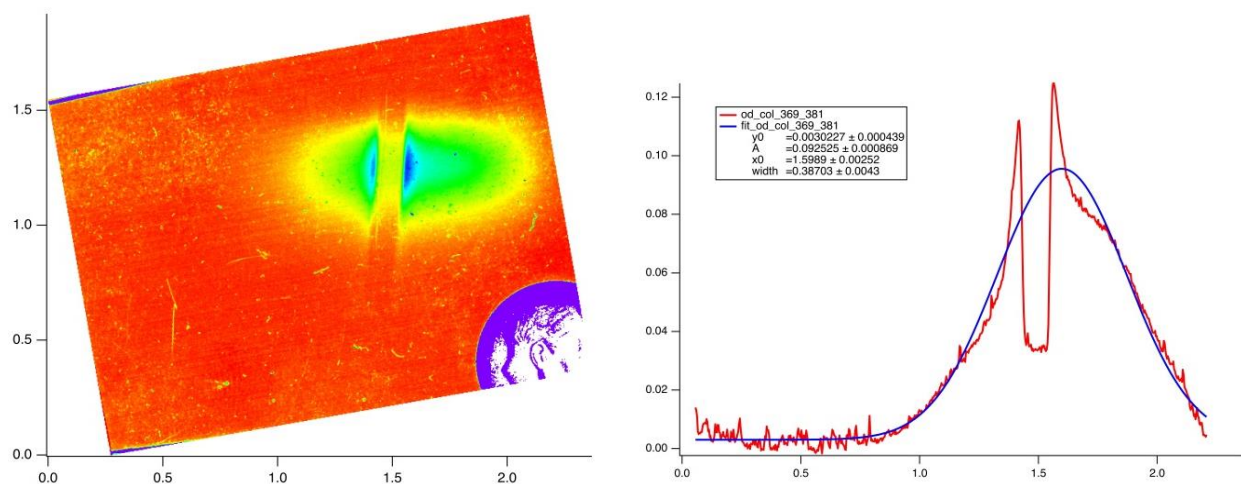


**FIGURE 5 (Left) Beam profile from scanned Plexiglas. Vertical line is shadow of target holder arm; all dimensions are in inches. (Right) Horizontal cross section of beam spot profile, intensity vs. inches.**

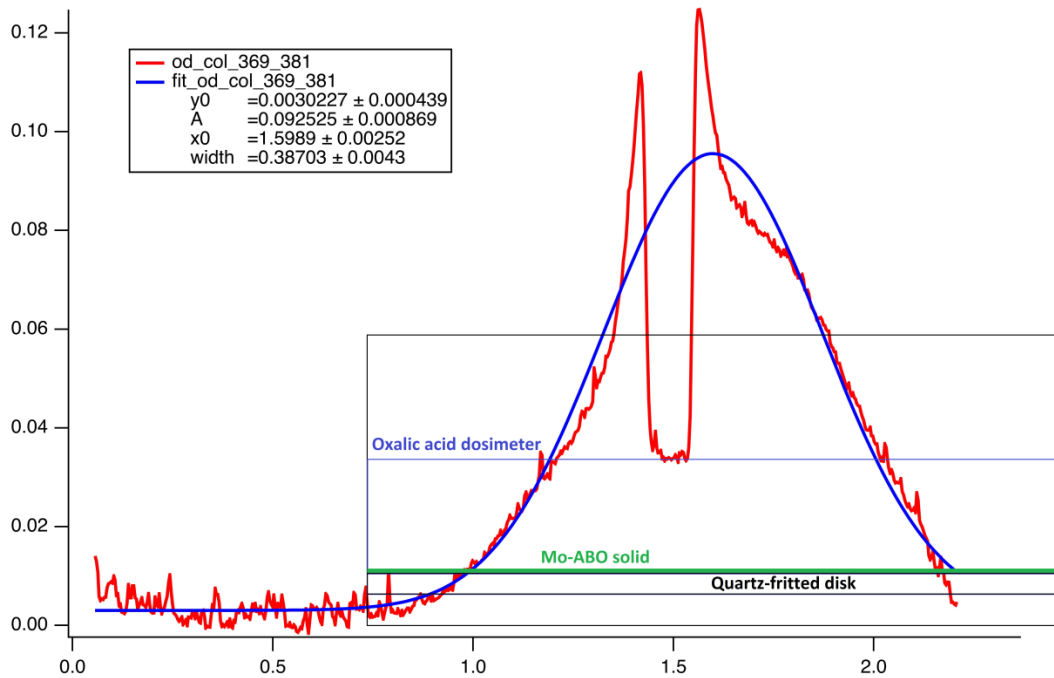


**FIGURE 6** Beam profile from scanned Plexiglas. Vertical line is the shadow of the target holder arm; all dimensions are in inches. Horizontal cross section of beam spot profile, intensity vs. inches with overlay of irradiation vessel. Irradiation vessel depicts approximate beam profile over vessel, the horizontal dimension of the vessel is to scale, the vertical dimension is not to scale.

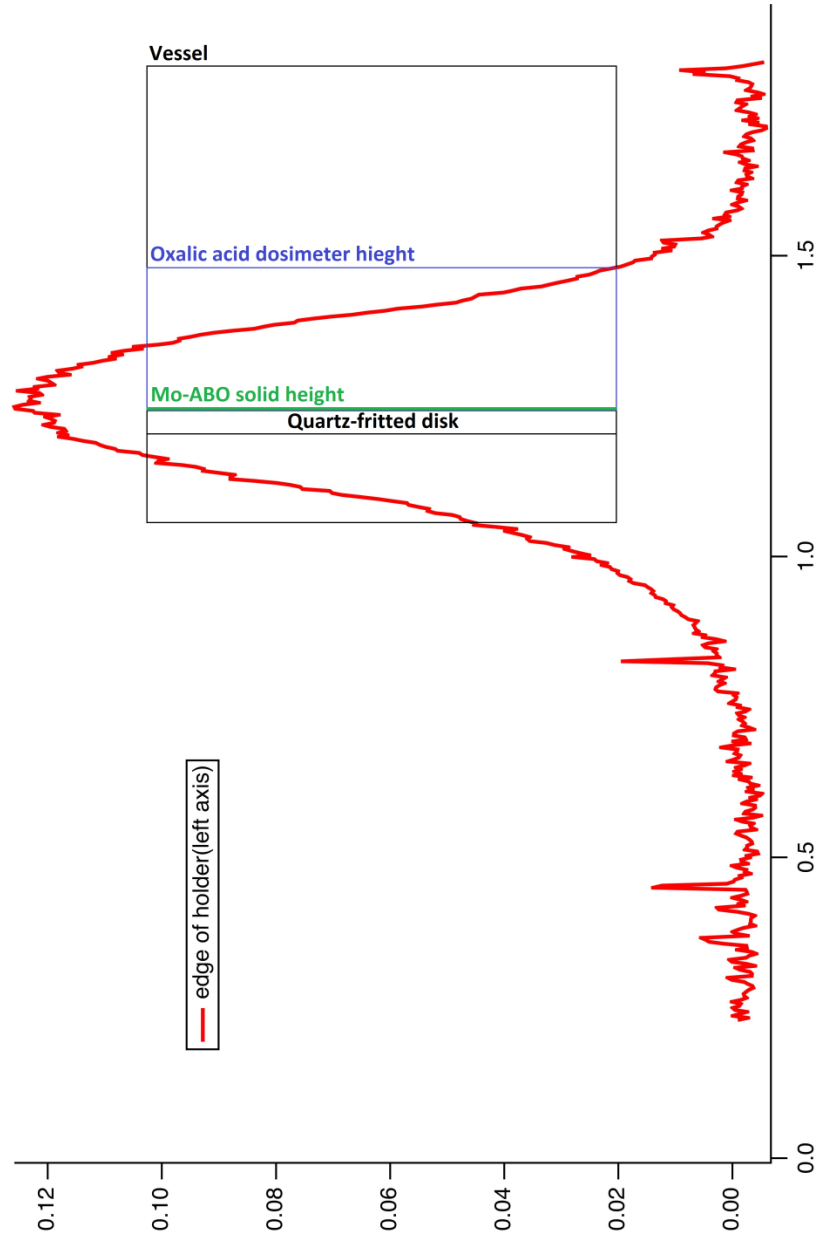


**FIGURE 7** Beam profile from scanned Plexiglas. Vertical cross section of beam spot profile, intensity vs. inches with overlay of irradiation vessel. Irradiation vessel depicts approximate beam profile over vessel, the vertical dimension of the vessel is to scale, the horizontal dimension is not to scale.

### 2.2.3 <sup>99</sup>Mo-ABO Linac Irradiation Rotation Rig

The irradiation vessel was essentially a quartz-fritted funnel with a diameter of 1.75 in. In order to distribute the intended dose evenly across the sample, the beam was defocused, and the sample was oscillated during irradiation. A simple motorized worm drive rotation stage (ThorLabs CR1-Z7) was utilized to provide rotation of the sample (Figure 8). The stage was remotely controlled with the associated software package supplied with the stage and set onto continuous rotation during irradiations. Sprockets were put in place on the mechanism and the shaft that held the sample in place during irradiation. The mechanism was placed ~3 feet below the irradiation vessel to minimize dose and risk of failure from exposure to radiation. This was later modified by replacing the chain with a drive shaft that provided 180° oscillation to the vessel as opposed to complete 360° rotation (Figure 9). The primary driver for the switch was the implementation of water cooling lines. Oscillating the vessel eliminated the possibility of the water lines coiling around the shaft holding the irradiation vessel.

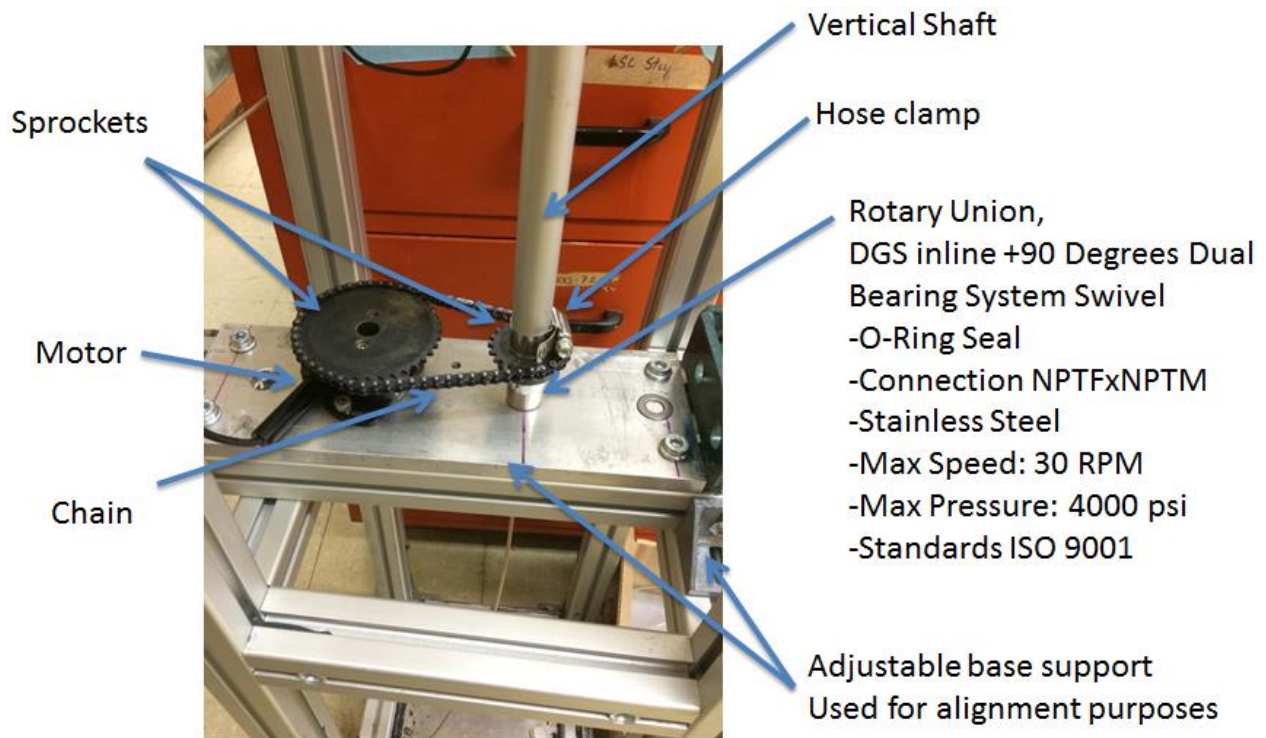


**FIGURE 8** Rotation mechanisms used to provide rotation of the sample during irradiation. Initial experiments utilized a drive chain. Other system components are depicted in the photo.

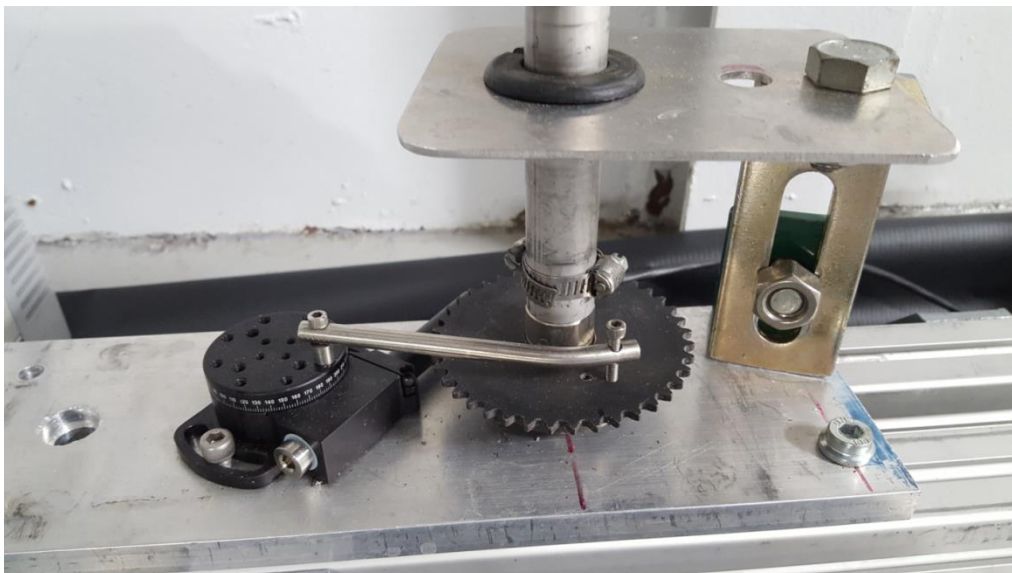


**FIGURE 9 Finalized designs utilizing a drive shaft that only provided 180° oscillation to allow for cooling lines**

Figure 10 depicts the vertical shaft and rotation system placed on a mock-beam line. The irradiation vessel shown in Figure 10 was later redesigned to allow for water cooling, shown in Figure 11. A hollow vertical shaft held the irradiation vessel in place during irradiation. Polyetheretherketone (PEEK) tubing (1/8 in.) was coiled into a spring and placed within the interior of the shaft. The spring was to allow for slack, ease of loading, and small alignment adjustments prior to irradiation. An Ultra-Torr vacuum fitting was used to make the seal between the quartz irradiation vessel and the PEEK tubing. Quartz was used instead of glass to minimize activation of the irradiation vessel. The samples required retrieval shortly after irradiation for processing purposes. Using quartz eliminated dose concerns while handling the vessels.

The PEEK tubing was connected to the system with compression fittings. A rotary union (DGS inline +90 Degrees Dual Bearing System Swivel) was used to create a water-tight seal at the base and allow for rotation of the vessel (Figure 10). A liquid transfer line was attached to the bottom of the structure to the opposite end of the rotary union. This line connected to the acid wash and vacuum system. The acid wash and vacuum systems were located inside of a small white glove box for secondary containment purposes (Figure 12). A dual syringe pump was utilized to inject the HNO<sub>3</sub> (0.1 M) wash solution into the irradiation vessel. The syringe system was able to hold a total of 260 mL of HNO<sub>3</sub> and was controlled by the associated software (SyringePumpPro – barrel size set to 50, flow rate set to 75 mL/min). The infusion volume was determined by combining the desired solution volume to be added to the vessel with the dead volume of the system. An exterior vacuum exhausted to the room exhaust system was used to remove the solution. The vacuum was on throughout the experiments, but a remotely operated valve was put in place to close it from the system. Two solenoid valves were used to close off one system (injection or vacuum) from the other. A schematic of the solution and exhaust lines is shown in Figure 13.

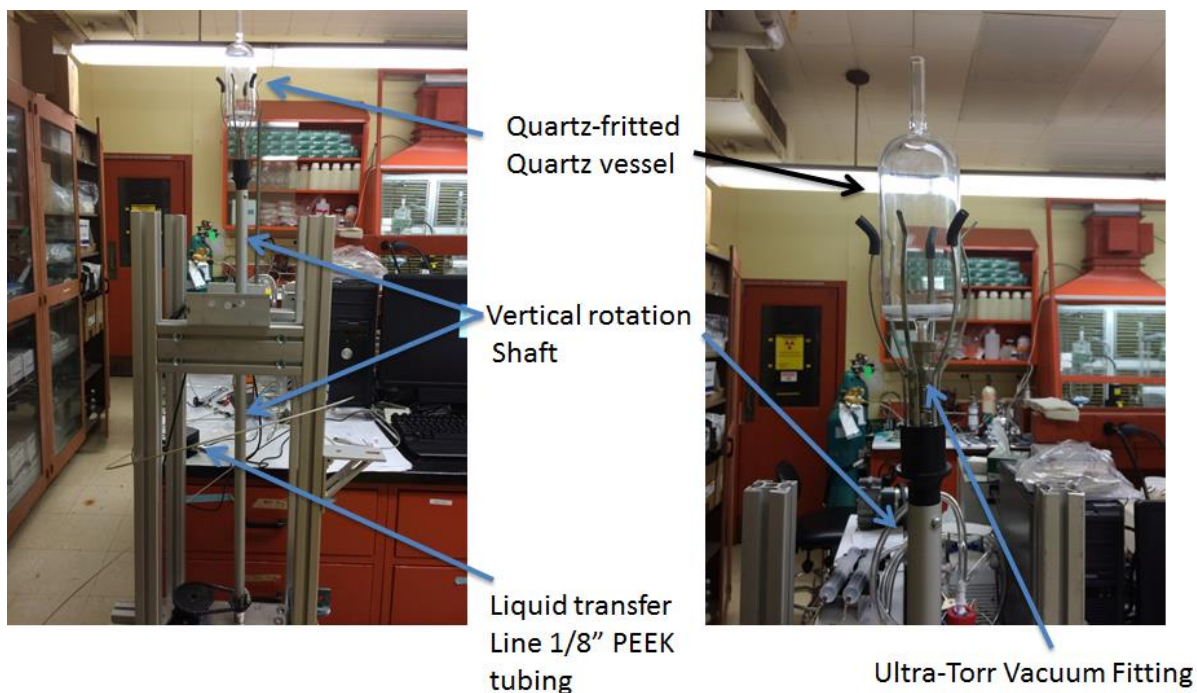


**FIGURE 10** Depiction of rotation system and mounted irradiation vessel on mock beam line



**FIGURE 11** Quartz irradiation vessels used during linac Mo-ABO trials. The vessels were quartz with a quartz-fritted funnel, and a quartz jacket for water cooling.

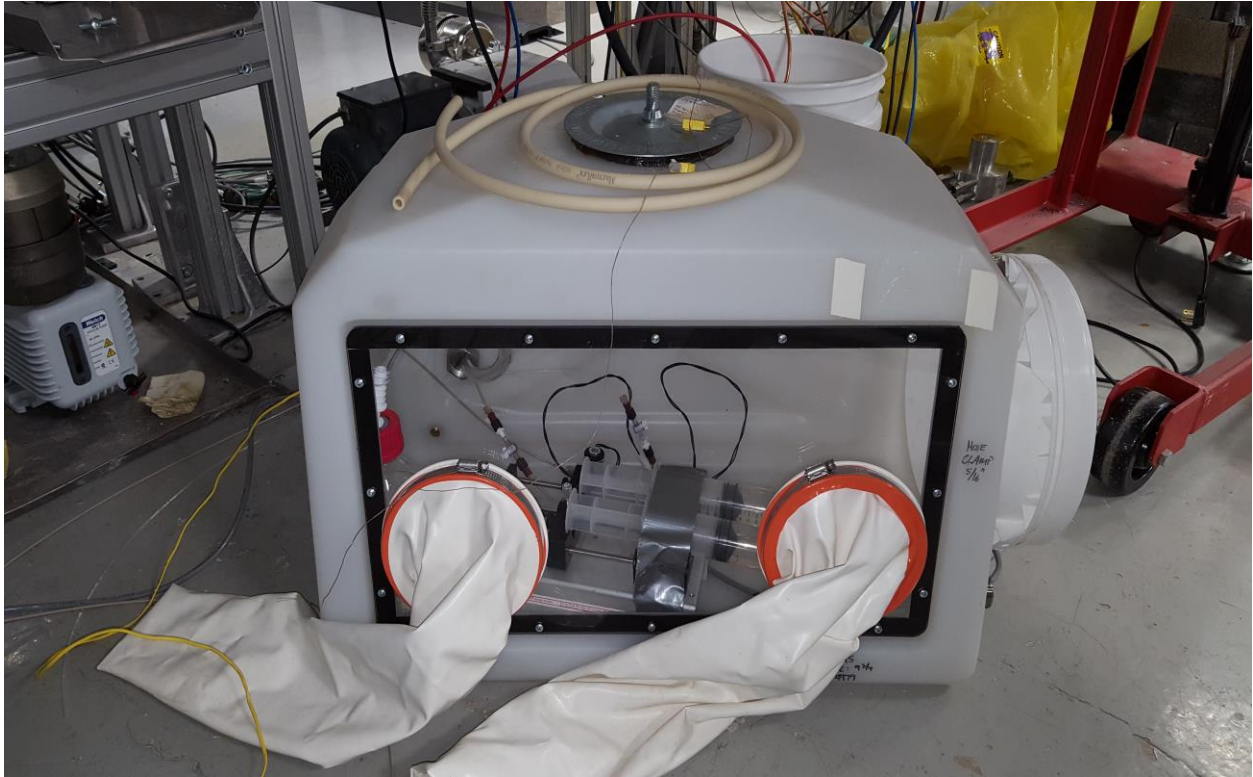


**FIGURE 12** Glove box used as secondary containment of the acid wash injection and vacuum systems

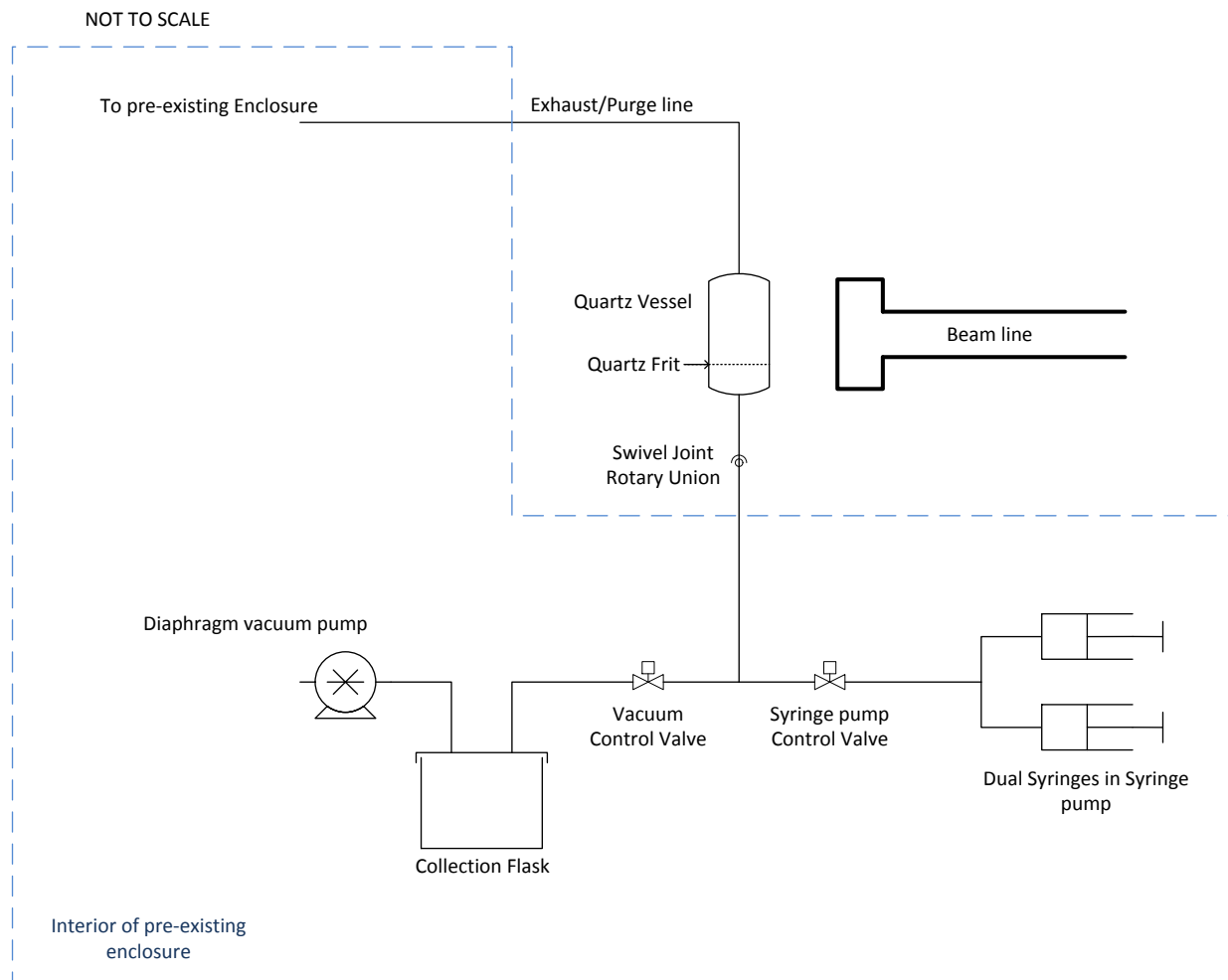


**FIGURE 13 Schematic drawing of linac experimental setup**

### 2.2.4 Linac Temperature Profiling

Temperature profiles during irradiation of the quartz irradiation vessel were investigated under dry and wet (20 mL of H<sub>2</sub>O) conditions with a thermocouple. The vessel was irradiated with an electron beam spread across the sample holder, as described in the beam-profiling experiments. A 35 MeV beam with various beam powers (3, 2, 1, and 0.5 kW) was investigated. The irradiations began under dry conditions. Water was introduced to the system during the irradiations under constant beam. Dry and wet conditions were alternated throughout the irradiations in order to determine the temperature changes that would occur under experimental conditions.

The vessel used during irradiation of the Mo-ABO complex was also utilized for the temperature studies in order to obtain data representative of actual conditions. A thermocouple was placed in the interior of the vessel during the irradiations. The vessel was rotated as in the Mo-ABO experiments. The experiments were performed with a 35 MeV beam with various

beam powers (3, 2, 1, 0.5 kW); the results are summarized in Figure 14. With a beam power of 3 kW, the temperature rose under dry conditions extremely quickly and to a maximum of 800°C before the beam was shut off. The thermocouple did not return to room temperature prior to irradiating the vessel with a 2 kW beam. Starting at ~300°C, the temperature rose to 500°C upon introduction of the 2 kW beam. The irradiation was again halted and the power brought to 1 kW. At 1 kW, the temperature under dry conditions reached 370°C. Water was introduced into the system to determine what temperature the system would reach under “wet” conditions. The solution boiled and began to level at ~110°C. The beam power was then decreased to 0.5 kW and the solution was irradiated. Under wet conditions, the temperature of the system leveled near 85°C. The solution was removed via vacuum, and the temperature of the system rose to 260°C and averaged ~255°C. This process was repeated to determine the average temperature of the system under the dry and wet conditions. The temperature quickly dropped upon addition of water to the system.

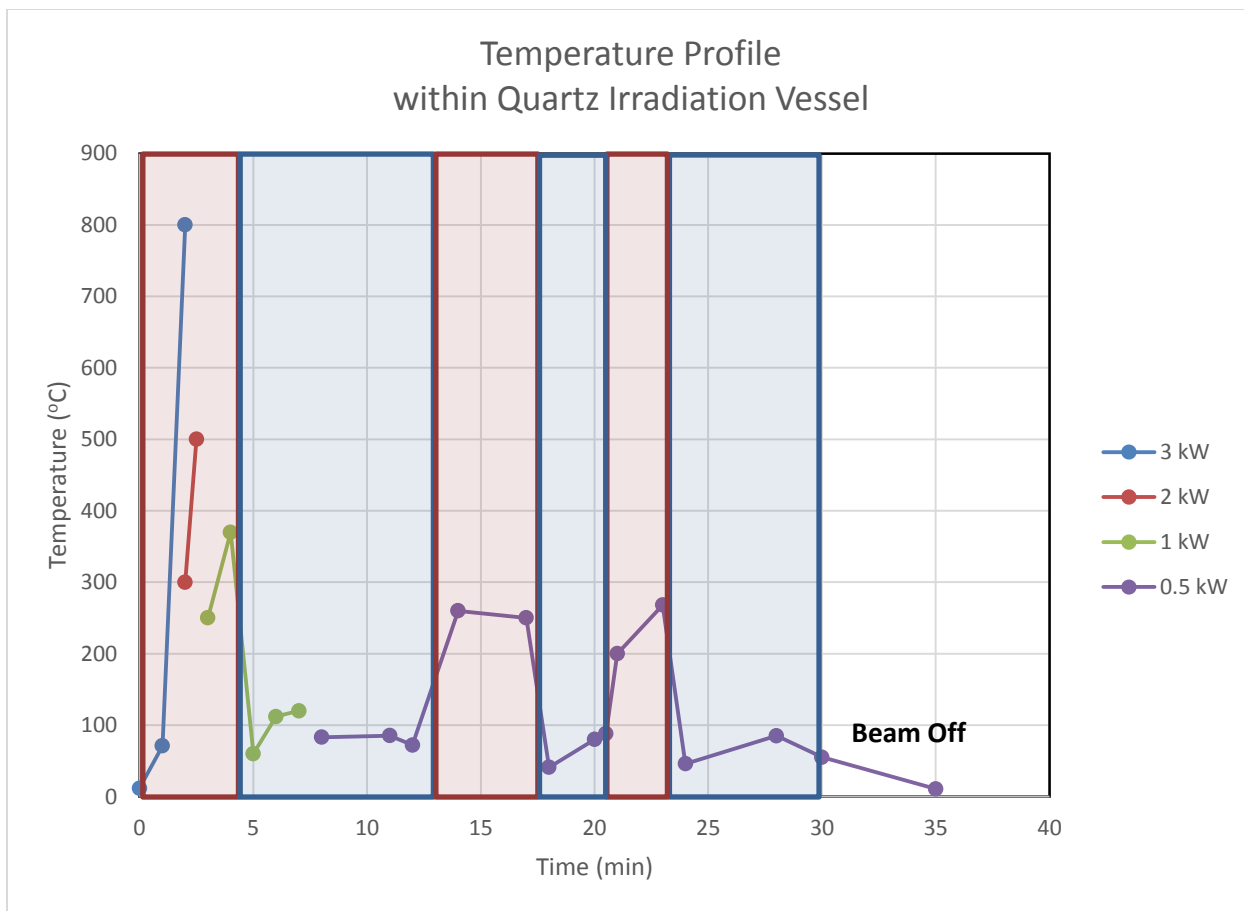


**FIGURE 14** Temperature profile of quartz vessel under dry (red/orange shaded regions) and wet (blue shaded regions) conditions

### 2.2.5 Linac Oxalic Acid Dosimetry

Doses were determined by oxalic acid dosimetry. A solution of oxalic acid (~0.6 M, 10 mL) was irradiated with a 35 MeV, 0.5 kW beam at 12 in. from a beryllium window for various time periods and cooled with a constant stream of compressed air (chilled by a salted ice bath). The clear quartz irradiation vessel darkened (purple in color) over time. Irradiated solutions of oxalic acid (1 mL of the 10 mL sample) were titrated with standardized NaOH to determine the final concentration of oxalic acid. Titration of the stock solution of oxalic acid was performed to determine the starting concentration of the oxalic acid. The results were plotted to obtain a linear dose curve. As stated previously, the received dose is extremely dependent on the position of the sample. Therefore, multiple irradiations were performed with a rotating rig. These data were combined and plotted to determine dose rates.

### 2.2.6 Linac <sup>99</sup>Mo-ABO Experiments

Molybdenum carrier solution (10 mg-Mo/mL) was prepared by dissolving MoO<sub>3</sub> in NaOH (1 M) and neutralizing it with HNO<sub>3</sub> (8 M). Prior to precipitation with ABO, the Mo carrier solution was spiked with a known amount of Mo-99. ABO (2%) was prepared by dissolution of ABO in hot NaOH (0.4 M). Molybdenum carrier (0.5 mL) spiked with Mo-99 was diluted with HNO<sub>3</sub> (~1.5 M, 50 mL) and oxidized with KMnO<sub>4</sub> (2.5% KMnO<sub>4</sub>, 1 mL). The resultant solution was mixed and then precipitated with the ABO stock solution (20 mL). The mixture was transferred by pipette into the irradiation vessel. Vacuum was applied and the solution was removed. The solid left on the frit was washed with HNO<sub>3</sub> (0.1 M, 10 mL).

The loaded irradiation vessel was placed on a rotating rig and irradiated with a spread beam from the linac. Irradiations were performed with beam energy of 35 MeV and beam power of 0.5 kW. Irradiations were performed for various lengths of time to achieve calculated doses. During irradiation, the solid was washed with several aliquots of 0.1 M HNO<sub>3</sub> in two different volume sets ( three 20 mL aliquots and five 10 mL aliquots). The required irradiation time was calculated based on the oxalic acid dosimetry trials. The irradiation time was evenly distributed between dry and wet conditions (i.e., 3.8 kCi = 32 min irradiation, 8 wet and 8 dry steps for a total of 16 steps, where Mo-ABO was dry for 2 min and then wet for 2 minutes; 6.2 kCi = 52 min irradiation, where Mo-ABO was dry for 3 min and 15 sec and then wet for 3 min and 15 sec).

### 3 RESULTS AND DISCUSSION

#### 3.1 VDG EXPERIMENTS

##### 3.1.1 VDG Oxalic Acid Dosimetry Verification

The dose received by Mo-ABO samples was determined by using oxalic acid. A direct relationship exists between the current and received dose (Figure 15, Table 1). To verify the behavior of the system used, dose measurements were determined at 50, 30, 10, and 5  $\mu\text{A}$ . The measured dose rates are shown in Figure 15 and tabulated in Table 1. The data indicate that the dose rate increases linearly with current. The current did not deviate during the oxalic acid irradiations, as they were relatively short, <30 minutes. However, the beam current changes over time during long experimentation. Therefore, a correction factor needed to be applied to the 8.382 Mrad/min conversion factor for long irradiations.

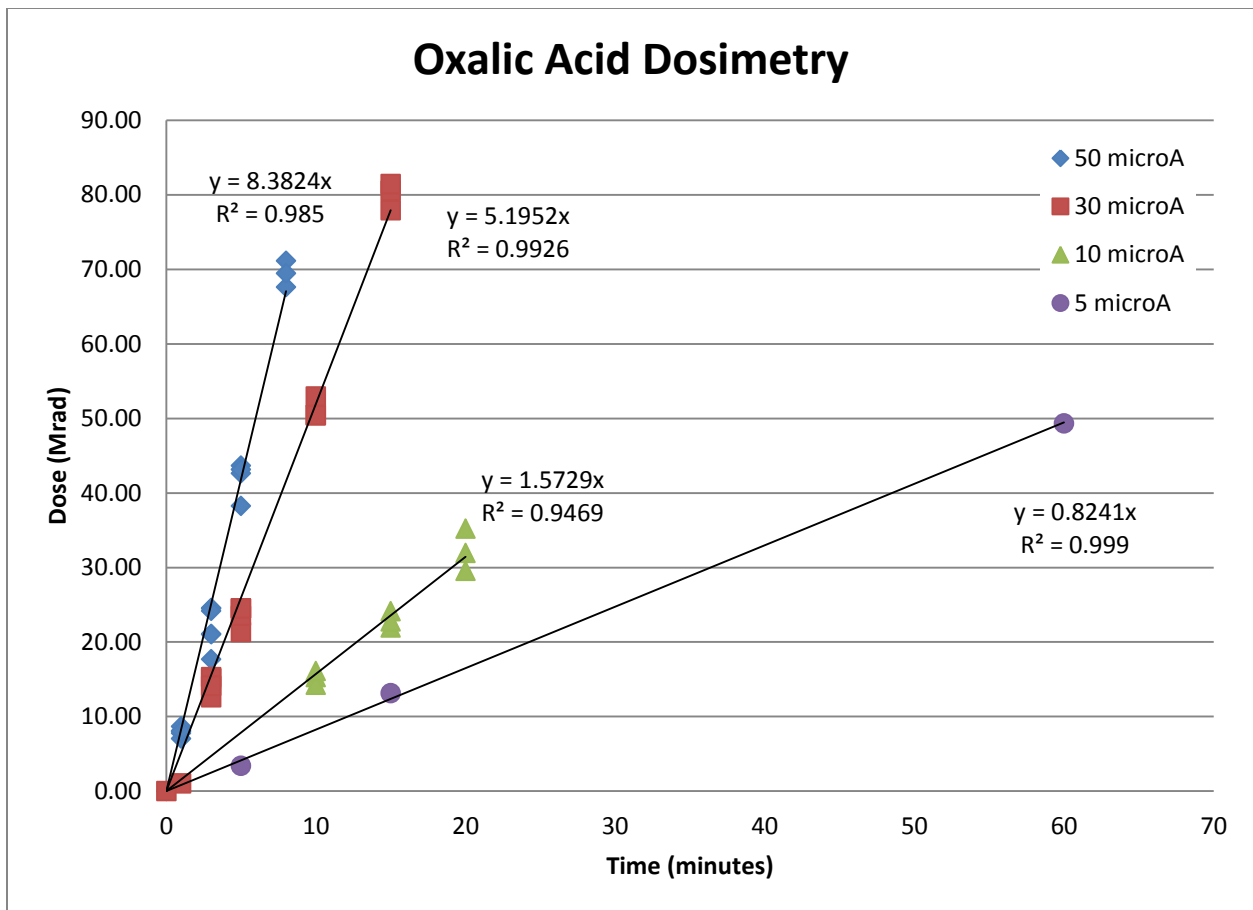


FIGURE 15 Oxalic acid dosimetry results at various beam currents

**TABLE 1 Dose rates attained with various beam currents used at 3 MeV VDG**

Current (μA)	Dose Rate (Mrad/hr)
5	0.824
10	1.57
30	5.19
50	8.38

### 3.1.2 VDG Correction Factor

The dose received by the Mo-ABO complex was determined by measuring the beam current on the aperture and relating this to the actual beam current (Figure 16). The current alters slightly throughout the course of the experiments. Therefore, a correction factor was applied to the calculated dose received by the Mo-ABO sample as determined by the oxalic acid dosimetry. The current of the beam was measured on the aperture during all experiments and throughout the breadth of the experiments. The currents measured over a single experiment were averaged over the entire experiment and used to apply a correction factor to the dose rates used to determine the dose received after an irradiation (Table 2).

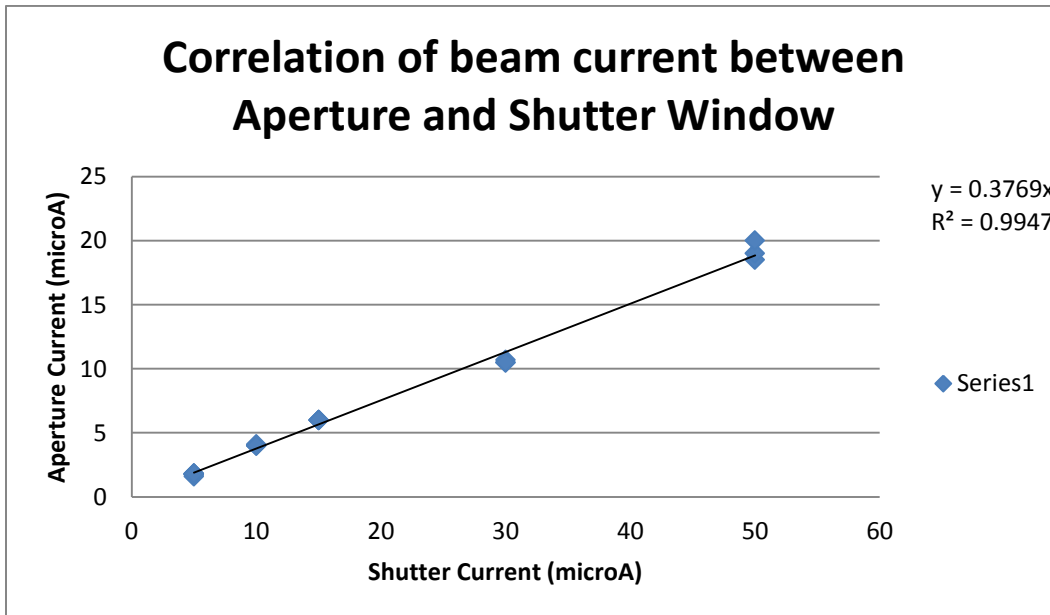


**FIGURE 16 Correlation of Van De Graaff beam current measured on the beam shutter window and the aperture. Measurements were taken with shutter fully closed and correlated to the aperture currents when the shutter was open. The sample receives dose while the shutter is open and receives no dose when the shutter is closed.**

**TABLE 2 Molybdenum-99 dose equivalents calculated with correction term to account for current variations during experiments**

Total Time (hr)	Expected Current from Shutter ( $\mu\text{A}$ )	Average Current on Aperture ( $\mu\text{A}$ )	Calculated Average Current on Shutter ( $\mu\text{A}$ )	Conversion Factor Determined from Oxalic Acid (Mrad/hr)	New Dose Factor (Mrad/hr)	Dose (Mrad)	Mo-99 Equivalence (kCi)
0.5	50	19.3	51.1	8.38	8.56	254	1.71
1.0	50	21.4	56.7	8.38	9.51	570	3.85
2.0	50	18.8	49.8	8.38	8.34	1,010	6.79
3.0	50	19.8	52.4	8.38	8.79	1,580	10.7
5.0	50	19.4	51.5	8.38	8.63	2,590	17.5
6.0	50	19.7	52.3	8.38	8.78	3,180	21.4
7.1	50	19.1	50.7	8.38	8.51	3,600	24.3
8.0	50	19.5	51.7	8.38	8.66	4,160	28.0

### 3.1.3 VDG <sup>99</sup>Mo-ABO Irradiations

Fresh Mo-ABO was prepared for each experiment. The white solid received calculated doses ranging from 254 to 4,156 Mrad. The white solid browned during shorter irradiations and blackened over longer irradiations. The data in Tables 3 and 4 and Figure 17 show the distributions of Mo-99 among the HNO<sub>3</sub> washes, NaOH product solution, and any residual left on the filter.

All samples showed signs of degradation after irradiation; colorless HNO<sub>3</sub> turned a light yellow, and the NaOH solutions were dark brown. Despite the discoloration of the HNO<sub>3</sub> wash, only a small portion of Mo was detected in this fraction up to 15 kCi Mo-99 dose equivalence, which correlates with previous irradiations [14–16]. Larger fractions of Mo were observed in these washes at doses >15 kCi Mo-99 equivalent. From the data in Table 4 and Figure 17, it is evident that at dose equivalence >15 kCi Mo-99, the decomposition of the Mo-ABO complex leads to soluble Mo in 0.1 M HNO<sub>3</sub>, which causes a noticeable decrease in Mo recovery. Nearly complete degradation of the Mo-ABO complex was achieved at 24 kCi equivalence of Mo-99. To verify destruction of Mo-ABO at dose equivalents >24 kCi Mo-99, an additional experiment was performed with 28 kCi dose applied. The results demonstrate that >80% of Mo-99 was found in the HNO<sub>3</sub> wash fractions, verifying breakdown of the Mo-ABO complex at doses >24 kCi Mo-99.

The current data agree well with previous data [15] up to 12.5 kCi Mo-99 equivalent doses. However, the previous data suggest that >80% of Mo-99 was retained within the Mo-ABO complex up to 22.9 kCi equivalence Mo-99. The current data demonstrate ~80% recovery of Mo-99 at 17 kCi Mo-99, significantly lower than the previous data.

**TABLE 3 Recovery of Mo-99 activity in the HNO<sub>3</sub> wash, NaOH product solution, and residual left on the filter**

Mo-99 Equivalence (kCi)	Starting Activity ( $\mu$ Ci)	Activity from HNO <sub>3</sub> Wash ( $\mu$ Ci)	Activity from Filter ( $\mu$ Ci)	Activity from NaOH Solution ( $\mu$ Ci)
1.71	10.6	0.29	0.90	10.6
3.85	10.7	0.87	0.11	10.38
6.79	10.8	1.22	1.31	9.80
10.7	4.37	0.58	0.20	3.78
17.5	12.7	3.22	0.54	10.5
21.4	3.56	1.53	0.06	2.10
24.3	1.63	1.49	0.02	0.20
28.0	2.20	1.80	---	0.54

**TABLE 4 Measured percentages of Mo-99 recovered in the HNO<sub>3</sub> wash, NaOH product solution, and residual left on the filter**

Mo-99 Equivalence (kCi)	Starting Activity ( $\mu$ Ci)	% in HNO <sub>3</sub>	% on Filter	% in NaOH	Total (%)
1.71	10.6	2.70	8.54	100	111
3.85	10.7	8.19	1.07	96.4	105
6.79	10.8	11.4	12.1	91.0	114
10.7	4.37	13.4	4.47	86.4	104
17.5	12.7	25.4	4.28	82.6	112
21.4	3.56	42.9	1.72	59.1	103
24.3	1.63	91.2	1.07	12.1	104
28.0	2.20	81.8	—	24.6	106

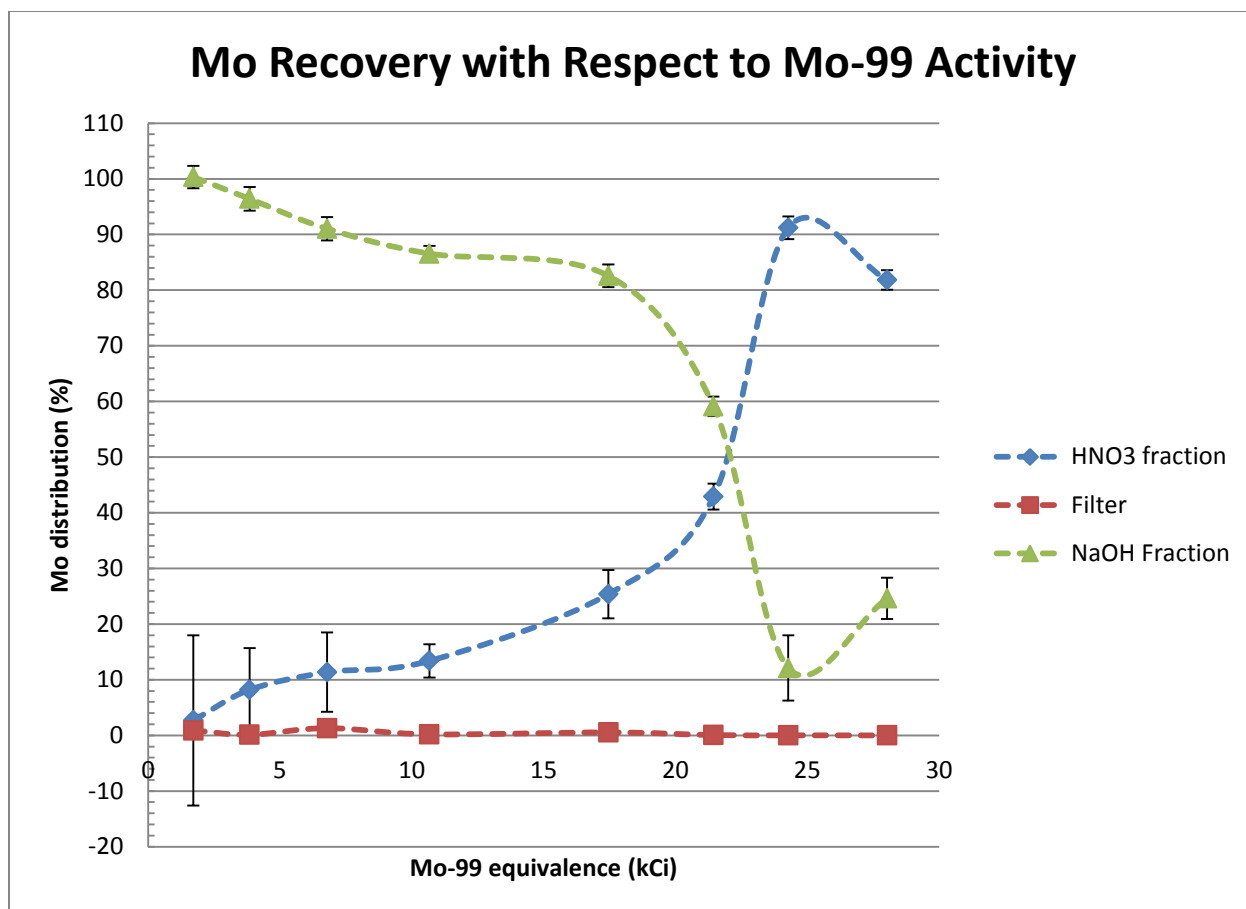


**FIGURE 17 Molybdenum recovery after applying a calculated dose of radiation with the VDG**

The data represented in Table 4 and Figure 17 have been condensed in Table 5 to demonstrate the amount of Mo-99 that was recoverable compared to that which was lost during processing after the receiving dose. Activity that was left on the filter and collected in the NaOH fractions was considered “recoverable.” Therefore the percent recoverable was the combination of the activity found on the filter and the NaOH fraction. Lost Mo-99 was the activity found in the HNO<sub>3</sub> washes.

In attempts to optimize the experimental procedure, samples were prepared 24 hours in advance. It was found that during the course of these experiments, samples prepared in advance demonstrated less stability to irradiation than freshly prepared samples. This developed a concern, as experiments performed with freshly prepared Mo-ABO at the VDG ranged from 50 minutes to 8 hours. Therefore, a study was performed to determine the stability of the Mo-ABO complex with respect to time. Samples were prepared as previously described. These samples were placed in a dark area (ABO is light-sensitive) for set periods of time. The results are shown in Figure 18. These studies found that the stability of Mo-ABO complexes does have a time dependency. Significant breakdown does not occur until after 144 hours of rest. This is outside the irradiation time periods set for this experiment. It is of note that as much as 10% Mo-99 can be lost even after 4 hours of rest.

**TABLE 5 Recoverable and loss of Mo-99 relative to Mo-99 dose equivalence**

Mo-99 Equivalence (kCi)	Dose (Mrad)	% Mo-99 Recoverable	% Error	% Mo-99 Lost	% Error
1.71	254	108	5.7	2.70	15.3
3.85	571	97.5	5.1	8.19	7.5
6.79	1,010	103	2.0	11.4	7.1
10.7	1,580	91.0	3.9	13.4	3.0
17.5	2,590	86.8	8.1	25.4	4.3
21.4	3,180	60.8	7.8	42.9	2.4
24.3	3,600	13.1	3.7	91.2	1.7
28.0	4,160	24.6	19.6	81.8	2.1

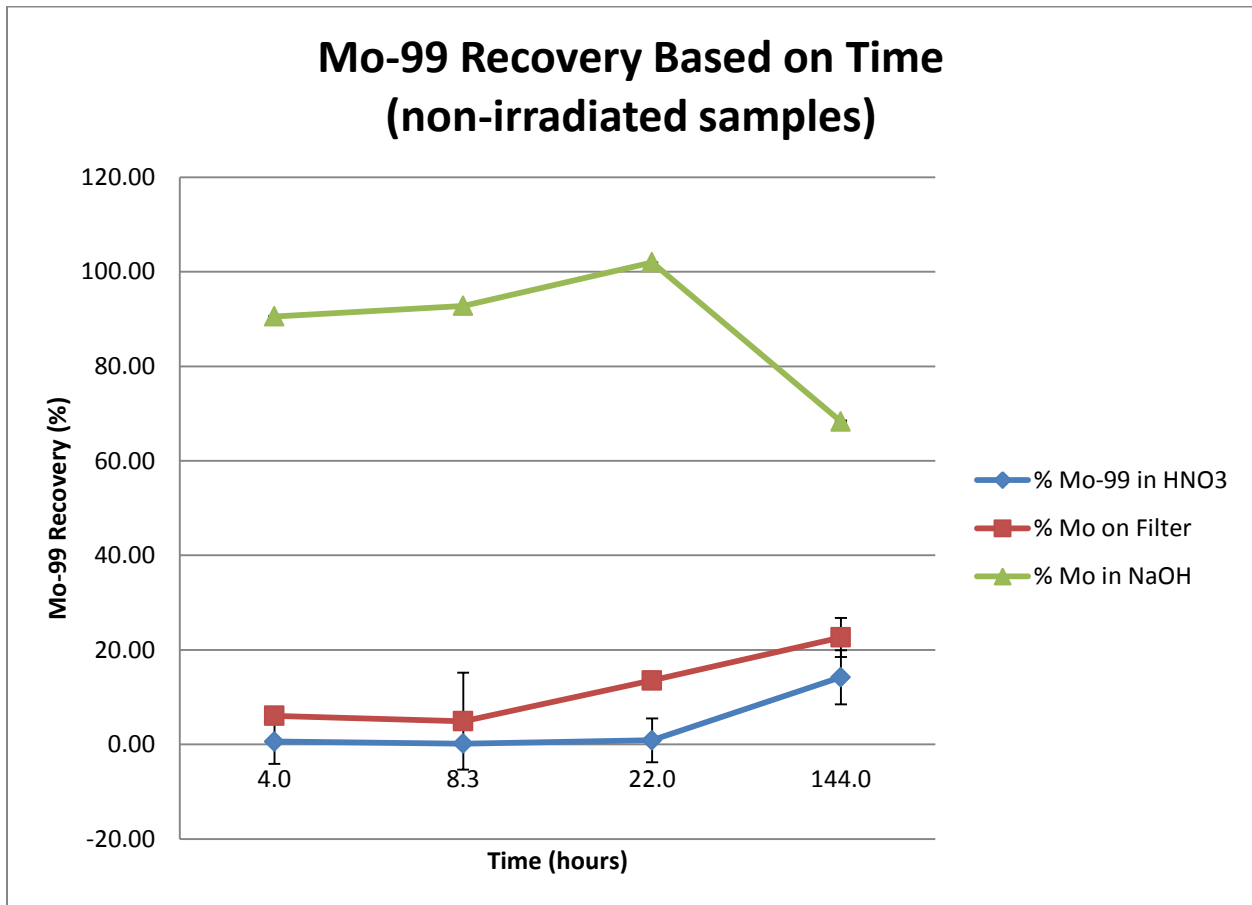


**FIGURE 18 Mo-ABO recovery based on age of non-irradiated samples**

## 3.2 LINAC EXPERIMENTS

### 3.2.1 Linac Oxalic Acid Dosimetry

Doses were determined by oxalic acid dosimetry. Solutions of oxalic acid (~0.6 M, 10 mL) were irradiated with a 35 MeV, 0.5 kW beam at ~12 in. away from the beam window. The samples were cooled with the water-jacketed quartz vessel during these initial trials. Multiple trials were performed in order to determine dose rates per electron beam pulse. The results of these trials are shown in Figure 19.

Extrapolation of the data to 6,000 Mrad provided insight into the number of pulses required to achieve up to 50 kCi dose equivalence of Mo-99 (Figure 20). From the data obtained during the VDG experiments, ~25 kCi Mo-99 or ~3,600 Mrad of dose would be required to destroy the Mo-ABO complex. During the linac trials, Mo-ABO experiments were planned ranging from 5 to 50 kCi Mo-99 equivalence. Table 6 details the correlation between Mo-99 equivalent dose and actual dose to irradiation time.

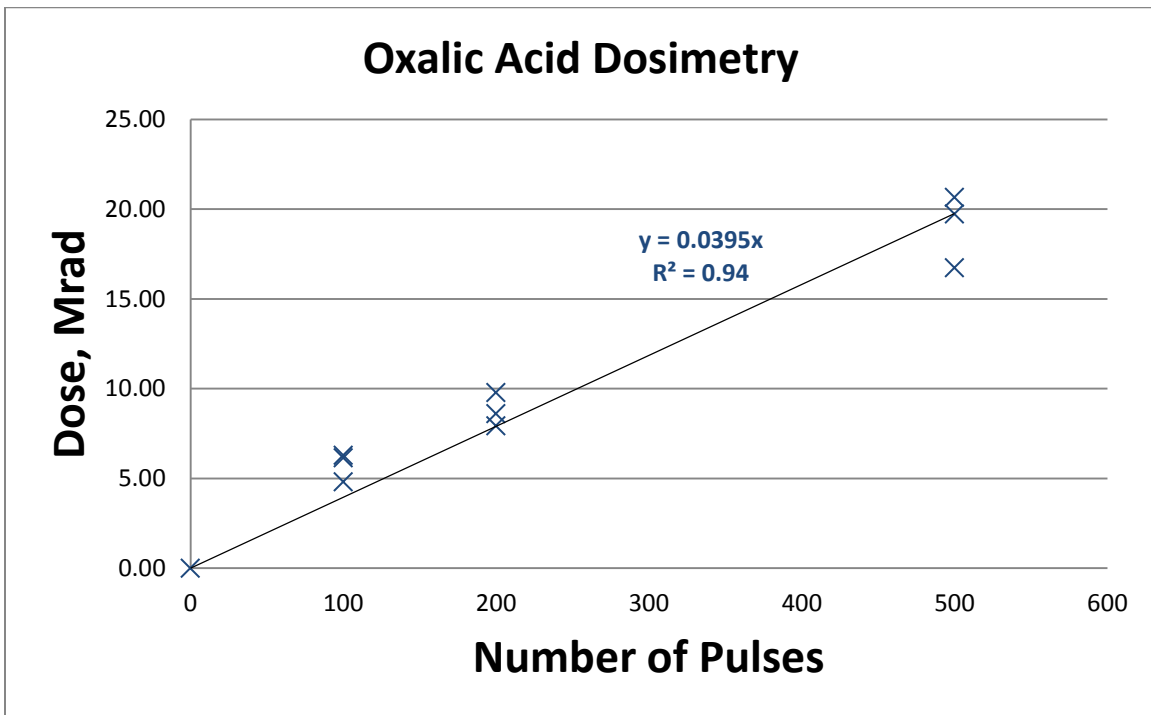


**FIGURE 19** Oxalic acid dosimetry curve obtained at 12 in. from the beam exit window. A 35 MeV beam with 0.5 kW of power at 5 Hz was used during these irradiations.

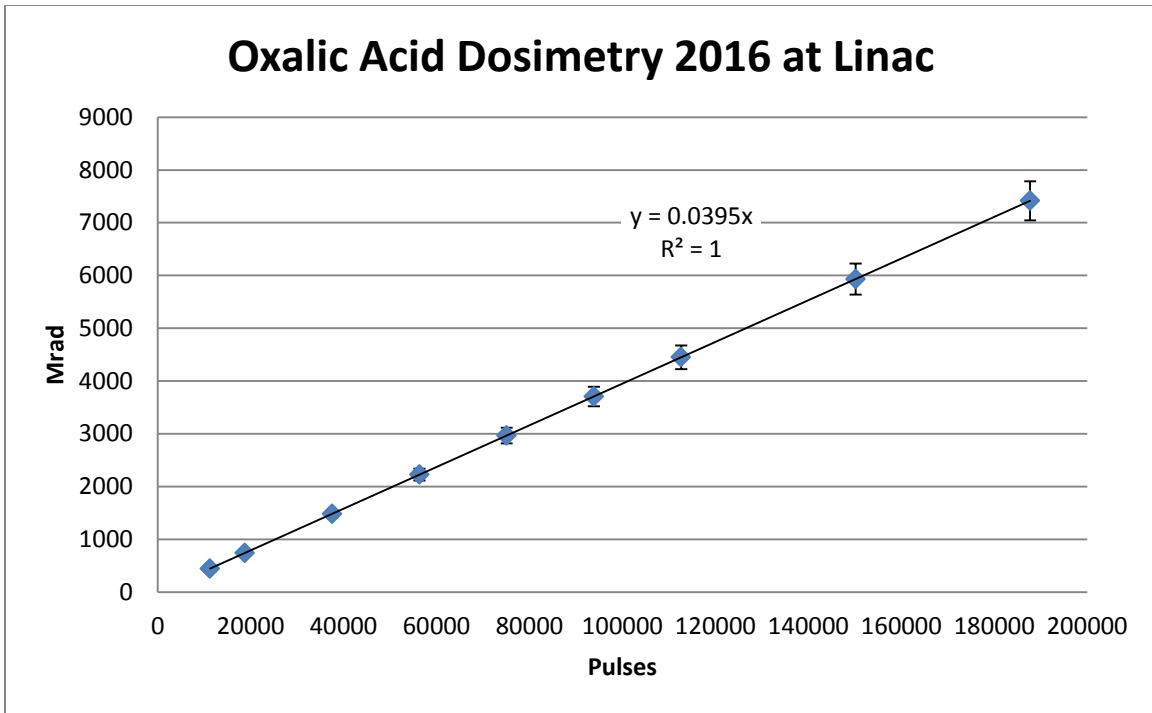


**FIGURE 20** Extrapolation of oxalic acid dosimetry to >7,000 Mrad. Error bars represent  $\pm 10\%$  error in dose.

**TABLE 6** Table relating Mo-99 dose equivalence as determined from oxalic acid dosimetry to Mo-ABO with geometric variable included\*

Mo-99 Dose Equivalent to Oxalic Acid (kCi Mo-99)	Actual Dose to Mo-ABO (Mrad)*	Irradiation Time (min)
3.8	556.4	31.3
6.2	926.1	52.1
12.5	1853.9	104.3
31.2	4633.9	260.7

\*Beam parameters: 35 MeV, 0.5 kW, 5 Hz.

### 3.2.2 Linac $^{99}\text{Mo}$ -ABO Experiments

Mo-ABO was prepared and irradiated as described above. The solid sample was freshly prepared before each experiment. Initial irradiations used quartz “beads” (more akin to cylinders) similar to the glass beads used in the LMC process (Figure 21). However, the quartz beads acted as a heat sink and did not help in the dissolution process during post-irradiation work-up of the samples. Significant amounts of Mo-ABO were charred and retained on the quartz beads after irradiation. Therefore, the quartz beads were removed from the system.

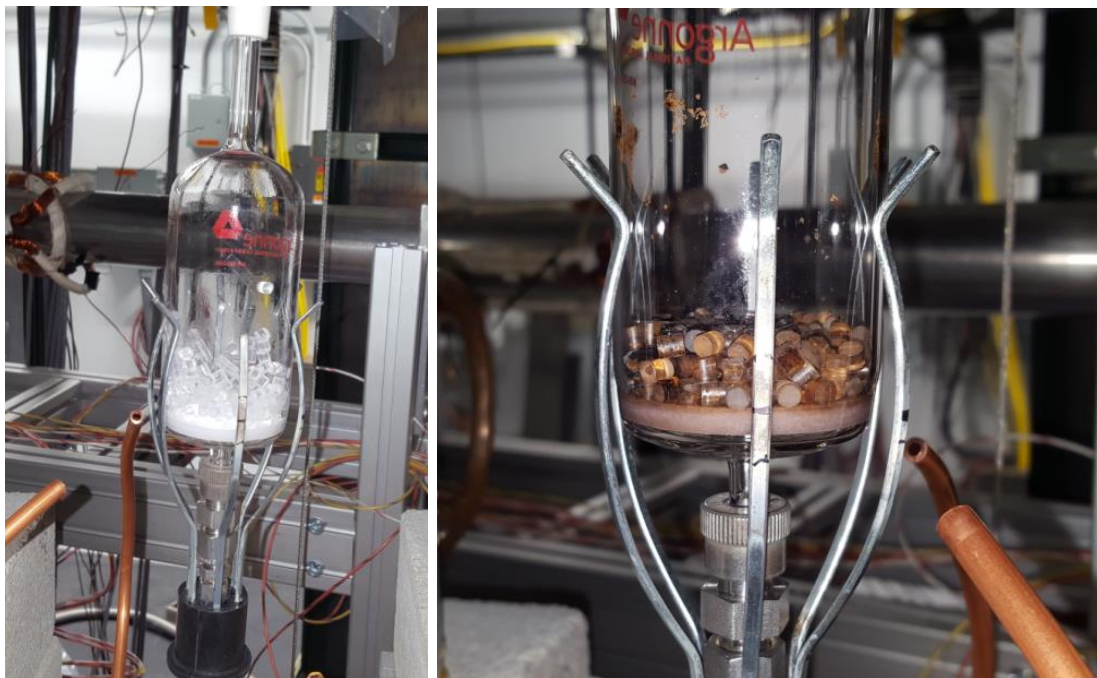


**FIGURE 21** Mo-ABO precipitated in a quartz irradiation vessel with quartz beads prior to irradiation (left), and Mo-ABO and quartz irradiation vessel with quartz beads after irradiation (right). Images are of the first version of the irradiation vessel. These vessels were initially used during full 360° rotation of the vessel. Jacketed vessels were used in the final version.

The first version of the irradiation vessel was replaced with a jacketed vessel to provide better cooling (Figures 9 and 22). Chilled water was supplied to the system by a recirculating bath set to 5°C. Figure 23 shows the irradiation setup. The quartz vessel was placed 12 in. away from the beam to allow for ample beam spread. Beam stops were used to collimate the beam to avoid irradiation of other system components. The beam was centralized on the frit so that the highest intensity region of the beam was just above the frit and struck the precipitated Mo-ABO. A water-cooled beam stop was placed after the irradiation vessel to completely stop the beam (Figures 24 and 25).

Prior to irradiation, the Mo-ABO solid appeared white, and the quartz vessel was clear and colorless. Post-irradiation, the Mo-ABO darkened and blackened under high dose conditions. The quartz vessel attained a purple hue. Interestingly, the purple color was only observed on the interior vessel and not on the exterior jacket (Figure 25). The darkening of the Mo-ABO solid was also observed in the VDG experiments (Figure 26) [15,16]. Discoloration of the HNO<sub>3</sub> wash solution was also noticed (Figure 27). The coloration did not have a direct link to activity (i.e., darker solutions did not necessarily mean that more Mo-99 was present due to the destruction of the Mo-ABO complex). This trait was also observed during VDG experiments [15,16].



**FIGURE 22 Jacketed quartz irradiation vessel with Mo-ABO precipitated on the frit. Cooling lines are shown in the image. Chilled water from a recirculating bath was introduced from the bottom and expelled from the top. A thin layer of Mo-ABO is almost invisible to the eye.**



**FIGURE 23** Mo-ABO precipitated in quartz vessel prior to irradiation. An aluminum window was used during these irradiations. The beam was spread with magnets and collimated with a lead brick and water-cooled beam stop. Hose clamps were used during all irradiations, not shown here.



**FIGURE 24** Alternative view of Mo-ABO precipitated in quartz vessel prior to irradiation. Water-cooled beam stops can be seen between the beam window and the irradiation vessel, as well as behind the irradiation vessel. Hose clamps were used during all irradiations, not shown here.



**FIGURE 25** Mo-ABO precipitated in quartz vessel after irradiation. The quartz darkened from exposure to the electron beam. Hose clamps are observed for the water cooling lines. Condensation can be seen on the exterior of the vessel. The condensation was from atmospheric water and does not represent a breach of containment.



**FIGURE 26** Discoloration of Mo-ABO solid (visible through the darkened quartz walls). The movement of the Mo-ABO solid from the frit was attributed to the introduction of the wash solution from the bottom of the vessel.

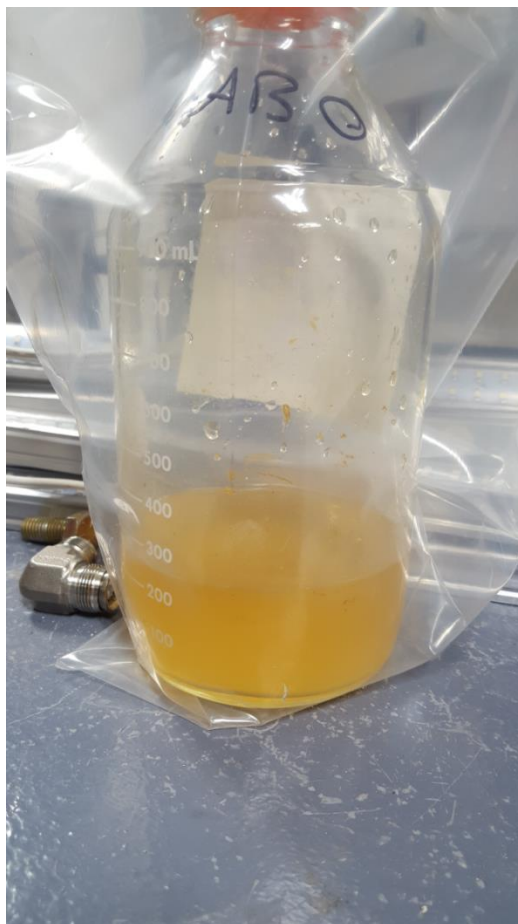


**FIGURE 27 Combined HNO<sub>3</sub> wash solutions post-irradiation. The coloration did not have a direct link to activity (i.e., darker solutions did not necessarily mean that more Mo-99 was present due to the destruction of the Mo-ABO complex)**

The Mo-ABO samples spiked with Mo-99 were irradiated and received a dose in the range ~556.4–4633.9 Mrad or equivalent of what would be expected from 3.8–31.2 kCi Mo-99. The data from these experiments are summarized in Tables 7 and 8. Post-irradiation, the irradiation vessel and the HNO<sub>3</sub> wash vessel were collected. The combined HNO<sub>3</sub> washes were counted with an HPGe detector. Irradiated Mo-ABO samples were dissolved with portions of NaOH (0.2 and 0.4 M, 20 mL) with H<sub>2</sub>O<sub>2</sub> (~1% total volume of NaOH solution). During the LMC process, the fritted bottle is subjected to direct heat with a heat gun. Direct heat on the jacketed vessel used here was not feasible; therefore, the NaOH solution was heated to a boil prior to addition to the quartz irradiation vessel. The vessel was held on its side so that the NaOH solution would not pass through the frit until desired. Hydrogen peroxide was then added to the hot NaOH in contact with the Mo-ABO. The solution immediately fizzed and bubbled. The vessel was swirled to dissolve as much of the Mo-ABO as possible prior to collecting the solution in a receiving vessel via vacuum filtration. On multiple trials, significant portions of the

activity remained on the frit along with portions of the undissolved solid. The NaOH fractions and frit were counted separately on an HPGe detector. The NaOH fractions also attained an orange-yellow coloration similar to that of the HNO<sub>3</sub> seen in Figure 27. Figure 28 shows a graphic representation of the distribution of Mo-99.

The irradiation vessels were stored for decay and future use. These vessels were washed with base, acid, peroxide, and water, and were gamma-counted prior to subsequent experiments. The residual solids were never completely removed from the fritted surface even though the washing was invasive and vigorous.

**TABLE 7 Distribution of Mo-99 activity in the HNO<sub>3</sub> wash, NaOH product, and residual on the frit**

Mo-99 Equivalent (kCi)	Actual Dose (Mrad)	Total Activity (μCi)	Activity in HNO <sub>3</sub> (μCi)	Activity in NaOH Fraction (μCi)	Activity Left on Frit (μCi)
3.8	556.4	63.2	4.99	5.92	34.6
6.2	926.1	183	38.9	21.2	36.4
12.5	1853.9	260	85.7	36.3	2.18
31.2	4633.9	52.5	21.7	4.65	5.58

**TABLE 8 Distribution of Mo-99 percentages in the HNO<sub>3</sub> wash, NaOH product, and residual on the frit**

Mo-99 Equivalent (kCi)	Actual Dose (Mrad)	% Activity in HNO <sub>3</sub> Fraction	% Activity in NaOH Fraction	% Activity on Frit	Total
3.8	556.4	7.91	37.3	54.8	99.7
6.2	926.1	21.2	59.0	19.8	100
12.5	1853.9	33.0	66.2	0.84	100
31.2	4633.9	41.3	48.1	10.6	100

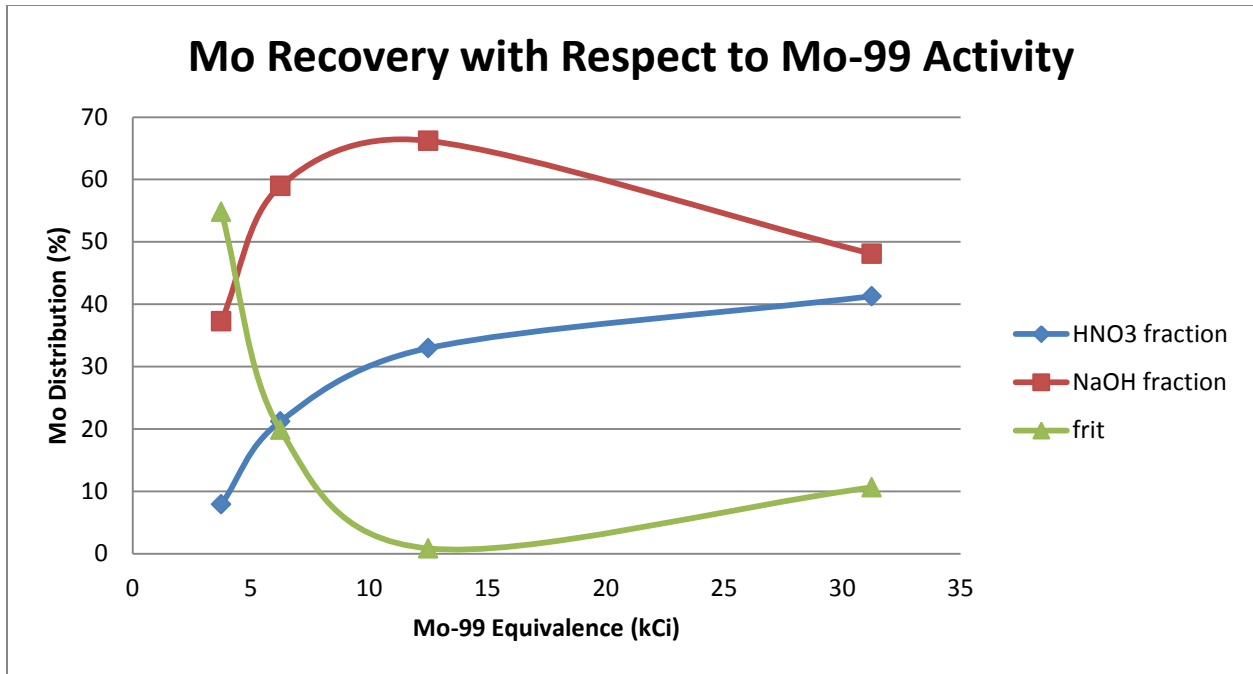


**FIGURE 28** Distribution of Mo-99 percentages in the HNO<sub>3</sub> wash, NaOH product, and residual on the frit

Molybdenum-99 activity left on the frit and recovered in the NaOH fraction can be considered as “recoverable” activity. As shown in Figure 28, the activity left on the frit varies from experiment to experiment with no correlation to dose, suggesting that the wash steps and not the dose received was the reason why activity was left on the frit. All activity found in the HNO<sub>3</sub> fraction is considered lost. Therefore, a trend can be seen comparing recoverable Mo-99 to lost Mo-99 (Table 9 and Figure 29).

**TABLE 9** Percent of Mo-99 recovered and lost from Mo-ABO linac experiments

Mo-99 Equivalent (kCi)	Actual Dose (Mrad)	% Recoverable	% Lost
3.8	556.4	92.1	7.9
6.2	926.1	78.8	21.2
12.5	1853.9	67.1	33.0
31.2	4633.9	58.7	41.3

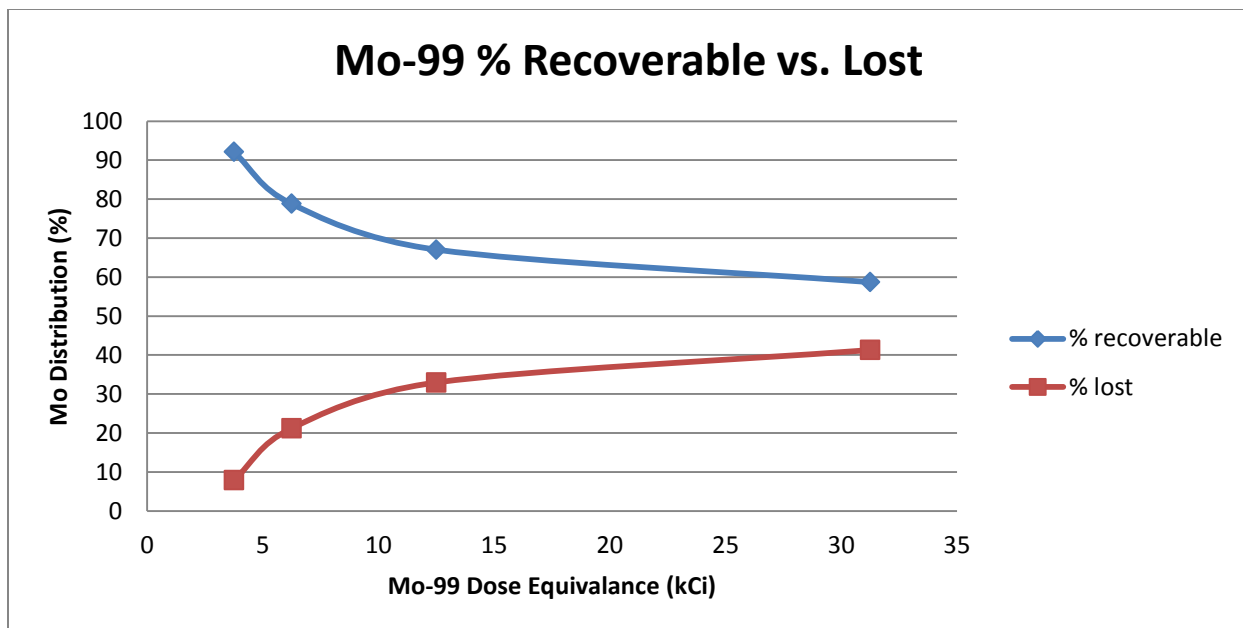


**FIGURE 29** Percent of Mo-99 recovered and lost in relation to Mo-99 equivalent dose

There is an obvious trend in lost Mo-99 compared to dose. Less than 10% of Mo-99 is lost at 3.8 kCi equivalent dose of Mo-99. The loss gradually increases as the received dose increases in the order 6.2, 12.5, and 31.2 kCi Mo-99 equivalent doses. The loss of Mo-99 plateaued and leveled between 12.5 and 31.2 kCi Mo-99; this is in stark contrast to the VDG trials, where the loss of Mo-99 increased drastically at doses >15 kCi. More than 80% loss of Mo-99 was observed at 25 kCi Mo-99 during the VDG experiments, while <40% was lost at the same dose equivalence during the linac experiments. This may be attributed to the heat deposited in the sample during these irradiations.

During VDG trials, Mo-ABO was always under wet conditions, covered with HNO<sub>3</sub> (0.1 M), and the temperature never rose above 25°C, while the temperature rose >250°C during dry conditions and between 80 and 90°C under wet conditions at the linac. Significant blackening of the Mo-ABO solid occurred during the linac trials. This was most likely an indication that the Mo-ABO complex was being thermally decomposed. During thermal decomposition, the organic complex may be forming an intractable decomposition product that behaves as a protective barrier that does not readily release Mo-99 to the HNO<sub>3</sub> washes. The solid also showed resistance to dissolution under NaOH/H<sub>2</sub>O<sub>2</sub> conditions. Also, HNO<sub>3</sub> washes performed on VDG-irradiated Mo-ABO made use of a vortex mixer while the washes performed during linac irradiations simply covered Mo-ABO with HNO<sub>3</sub> with no agitation. This may provide another possible explanation to the stark difference in the Mo-99 recoveries in the VDG and linac experiments.

The increased heat deposited in the Mo-ABO sample may also explain why there was relatively no change in loss of Mo-99 at 3 dose equivalents of Mo-99 between the VDG and linac experiments and a stark difference at 6 dose equivalents of Mo-99. The linac experiments

were performed in such a way that the time the Mo-ABO was under wet and dry conditions was equal. For the 3.8 kCi = ~32 minute irradiation (8 wet and 8 dry steps for a total of 16 steps), Mo-ABO was dry for ~2 min and then wet for ~2 min; for the 6.2 kCi = ~52 min irradiation, Mo-ABO was dry for ~3 min and 15 sec and then wet for ~3 min and 15 sec. During the temperature profiling experiments at 0.5 kW, the temperature of the thermocouple rose from 80°C to 200 °C in less than a minute. However, this may not reflect the temperature rise of the Mo-ABO solid. It may require more time to reach its maximum temperature than the thermocouple indicated. This relationship is true for metals (thermocouple) vs. ceramics and salts (Mo-ABO). It is possible that the Mo-ABO did not reach its thermal decomposition temperature during the 5.8 kCi (2 min dry time) run, but may have begun to or have reached it during the 9.7 kCi (3 min 15 sec dry time) run, 19.4 kCi (6 min 33 sec dry time) run, and 48.5 (16 min 15 sec dry time) kCi run. This may account for the gradual loss of Mo-99 during linac studies, as opposed to the dramatic loss of Mo-99 during VDG studies.

The actual heat that would be applied to the Mo-ABO solid from Mo-99 emissions was determined with Equation 1 [21]:

$$P = 1.6 \times 10^{-13} \frac{E \lambda A_v}{M} \quad (1)$$

where P is the power in thermal watts generated as heat,  $1.6 \times 10^{-13}$  is a conversion factor, E is the emission energy,  $\lambda$  is the decay constant,  $A_v$  is Avogadro's number, and M is the atomic weight in amu. With this equation, the thermal power expected from the maximum beta emission (1.214 MeV) of Mo-99 is 3,433 W(thermal)/g of Mo-99. This is an extreme overestimate of the thermal power generated by Mo-99. If instead the most abundant average beta energy (0.443 MeV, 82.2% abundant) is used, the thermal power expected from the decay is 1,258 W(thermal)/g. Table 10 shows the mass of Mo-99 expected from various activities of Mo-99 and the change in temperature expected in 20 mL of water from the heat given off from the beta emission. Water was chosen as an example scenario. This scenario assumes an adiabatic system where all of the energy released by the beta emission is retained and deposited in the system, and none of the heat is distributed to the environment.

The specific heat of Mo-ABO is unknown, and thus it is currently impossible to determine the actual temperature rise of the Mo-ABO complex itself under dry conditions. However, if the change in temperature predicted in Table 11 is extrapolated over several minutes, the temperature rise does not begin to reach the levels of those seen during the linac experiments until 25 kCi Mo-99 or until after 10 minutes of time. During the LMC process, each wash step generally requires less than 2 minutes to complete. Addition of fresh room-temperature solution will provide a medium in which the heat from the radioactive emissions can be deposited. Further, in a real scenario, not all of the emission will be absorbed by the system, the system will not be under ideal (adiabatic) conditions, and heat will be deposited into the environment. Therefore, it is unlikely that temperatures near the decomposition point of the Mo-ABO complex will be reached under normal conditions.

**TABLE 10 Data used to determine the change in temperature for various activities of Mo-99**

Activity (Ci Mo-99)	Mo-99 (g)	Power from Beta Emission (W/g)	Energy (J/s)	Mass of Water (g)	Specific Heat (J/g°C)	Delta T (°C/s)
3,000	6.3E-03	3,433	2.2E+01	20	4.186	0.26*
5,000	1.0E-02	3,433	3.6E+01	20	4.186	0.43
6,000	1.3E-02	3,433	4.3E+01	20	4.186	0.51
10,000	2.1E-02	3,433	7.2E+01	20	4.186	0.86
25,000	5.2E-02	3,433	1.8E+02	20	4.186	2.1

\*Delta T for average beta emission for 3,000 Ci of Mo-99 is 0.09°C/s.

**TABLE 11 Temperature increases of various activities of Mo-99 over several time periods assuming complete deposition of the maximum beta emission in an adiabatic system**

Activity (Ci Mo-99)	Delta T (°C/s)	Temperature Rise at Time x, °C			
		1 min	2 min	5 min	10 min
3,000	0.26	15	31	77	---*
5,000	0.43	26	51	---	---
6,000	0.51	31	62	---	---
10,000	0.86	51	---	---	---
25,000	2.1	---	---	---	---

\*--- represents boiling conditions.

## 4 CONCLUSIONS

Irradiations of Mo-ABO with a Mo-99 spike were performed at the Argonne National Laboratory Van de Graaff (VDG) generator and the electron linear accelerator (linac). The VDG studies were performed with a 3 MeV, 50  $\mu$ A beam on Mo-ABO samples covered with HNO<sub>3</sub>. Samples of Mo-ABO precipitated in a glass vial were cooled with multiple jets of cold compressed air. The temperature of the samples did not rise above 28 °C. Dose equivalents up to ~28 kCi of Mo-99 were applied. After irradiation, the Mo-ABO precipitate was filtered, washed with HNO<sub>3</sub>, then dissolved in a hot NaOH/H<sub>2</sub>O<sub>2</sub> mixture, and rinsed with NaOH. All washes, dissolutions, and rinses were gamma counted to determine Mo-99 content. The experimental data demonstrate good radiation stability of the Mo-ABO complex up to ~15 kCi dose equivalents of Mo-99. Nearly complete destruction of the Mo-ABO complex occurred at doses >24 kCi Mo-99.

The linac studies were performed with a 35 MeV, 0.5 kW beam on Mo-ABO samples under dry and wet conditions to better represent actual processing conditions. The samples were irradiated in jacketed quartz vessels and cooled with recirculating chilled water. Dose equivalents up to 31.2 kCi of Mo-99 were applied. After irradiation, the HNO<sub>3</sub> wash was collected and counted, the Mo-ABO was dissolved and counted, and the frit was counted. It was found that even at 6.2 kCi of Mo-99 equivalence of dose, the sample lost ~20% of Mo-99. The 20% loss of Mo-99 may be attributed to the heat deposited in the sample during irradiation. Complete destruction of the Mo-ABO complex was not achieved. This may be the result of inadequate mixing during the wash steps (not vigorous as in the VDG trials) or a protective barrier being formed during thermal decomposition of the complex.

It is difficult to directly compare the VDG and linac experiments to one another as the conditions were different. However, with the previous discussion in mind, the VDG data seem to be a better representation of the stability of the Mo-ABO complex to dose.

## ACKNOWLEDGMENTS

Work supported by the U.S. Department of Energy, National Nuclear Security Administration's Office of Defense Nuclear Nonproliferation, under Contract DE-AC02-06CH11357. Argonne National Laboratory is operated for the U.S. Department of Energy by UChicago Argonne, LLC.

## REFERENCES

- [1] S. Chemerisov, G.F. Vandegrift, "Mini-SHINE/MIPS Experiment," Argonne National Laboratory, ANL/CSE-14/2, September, **2011**.
- [2] A.J. Youker, D.C. Stepinski, L. Ling, N-H.L. Wang, G.F. Vandegrift, "Column Optimization for Mo Separation and Recovery," *Proceedings of the Mo-99 Topical Meeting on Molybdenum-99 Technological Development*, Washington, DC, USA, June 24–27, **2014**, S9–P9.
- [3] D.A. Rotsch, A.J. Youker, P. Tkac, D.C. Stepinski, J.F. Krebs, V. Makarashvili, M. Kalensky, Z. Sun, T.A. Heltemes, J.F. Schneider, A.S. Hebden, J.P. Byrnes, L. Hafenrichter, K.A. Wesolowski, S.D. Chemerisov, G.F. Vandegrift, "Chemical Processing of mini-SHINE Target Solutions for Recovery and Purification of Mo-99," *Proceedings of the Mo-99 Topical Meeting on Molybdenum-99 Technological Development*, Washington, DC, USA, June 24–27, **2014**, S9-P8.
- [4] D. Wu, B.A. Buchholz, S. Landsberger, G.F. Vandegrift, "Processing of LEU Targets for Mo Production—Testing and Modification of the Cintichem Process," *Proceedings of the XVIII International Reduced Enrichment for Research and Testing Reactors Meeting*, Paris, France, September 17–21, 1995, paper no. 3-3, May **1996**.
- [5] G. F. Vandegrift, C. Conner, G.L. Hofman, J.L. Snelgrove (ANL), A. Mutalib, B. Purwadi, H.G. Adang, L. Hotman, K. Moeridoen, A. Sukmana, T.J. Dicky, A. Sriyono, H. Suropto, D.L. Nasution, A. Amin, A. Basiran, S. Gogo, T. Taryo (PUSPIPTEK), "Demonstration of 99Mo Production Using LEU Metal-Foil Targets in the Cintichem Process," *Proceedings of the 22nd International Meeting on Reduced Enrichment for Research and Test Reactors*, Budapest, Hungary, October 3–8, **1999**.
- [6] C. Conner, J. Sedlet, T.C. Wiencek, D.J. McGann, G.L. Hofman, G.F. Vandegrift, J.L. Snelgrove (ANL, USA), A. Mutalib, A.H. Gunawan, H.G. Adang, H. Lubis, K. Wisnukaton, Kardarisman, A. Sukmana, Sriyono, B. Purwadi, D.T. Jatmiko, A. Suropto, D.L. Amin, A. Basiran, Martoyo, Sarwani, T. Taryo (BATAN, Indonesia), "Production of Mo-99 from LEU Targets--Acid-Side Processing," *Proceedings of the 2000 International Meeting on Reduced Enrichment for Research and Test Reactors*, ANL/TD/TM01-12, Argonne National Laboratory, July **2001**, p. 101.
- [7] D. Wu, S. Landsberger, G.F. Vandegrift, "Application of Neutron Activation Analysis in a Fission Molybdenum Separation Study," *J. Radioanal. Nucl. Chem.* 216:101-105, **1997**.
- [8] A. Elwell, *Analytical Chemistry of Molybdenum and Tungsten*, Pergamon Press, Oxford, New York, **1977**, pp. 40–41.
- [9] A. Parker, *Analytical Chemistry of Molybdenum*, Springer-Verlag, Berlin, New York, **1983**, pp. 146–147.

- [10] A.I. Busev, *Analytical Chemistry of Molybdenum* (translated by J. Schmorak), Ann Arbor, Humphrey Science Publishers, **1969**, pp. 30–31.
- [11] C. Conner, M.W. Liberatore, A. Mutalib, J. Sedlet, D. Walker, G.F. Vandegrift, “Progress in Developing Processes for Converting <sup>99</sup>Mo Production from High- to Low-Enriched Uranium–1998,” *1998 International RERTR Meeting*, Sao Paulo, Brazil, **1998**.
- [12] V. Makarashvili, S. Chemerisov, P. Tkac, G.F. Vandegrift, S. Zaijing, K.J. Quigley, G. Van-de-Graaff, “Dose Rate Calculations Irradiations for Testing Radiation Stability of Materials and Equipment,” *Proceedings of the Mo-99 Topical Meeting on Molybdenum-99 Technological Development*, Washington, DC, USA, June 24–27, **2014**, S9-P5.
- [13] I. Draganic, “Oxalic Acid: The Only Aqueous Dosimeter for In-Pile Use,” *Nucleonics*, 33–35, **1963**.
- [14] A.J. Youker, P. Chung, P. Tkac, K.J. Quigely, V. Makarashvili, D.L. Bowers, S.D. Chemerisov, G.F. Vandegrift, “Separation, Purification, and Clean-Up Developments for MIPS and SHINE,” *Proceedings of the Mo-99 Topical Meeting on Molybdenum-99 Technological Development*, New Mexico USA, December 4–7, **2011**, S11-P4.
- [15] P. Tkac, D.A. Rotsch, K. Quigley, G.F. Vandegrift, “Scalability of the LEU-Modified Cintichem Process,” Argonne National Laboratory, ANL/CSE-14/32, October, **2014**.
- [16] D.A. Rotsch, P. Tkac, S. Chemerisov, V. Makarashvili, K. Quigley, R. Gromov, L. Hafenrichter, G.F. Vandegrift, “Scalability of the LEU-Modified Cintichem Process,” *Proceedings of the Mo-99 Topical Meeting on Molybdenum-99 Technological Development*, Boston, USA, August 31-September 3, **2015**, S9-P7.
- [17] R. Gromov, K. Alford, D. Brown, S. Chemerisov, S. Forknall, J. Gardner, L. Hafenrichter, C.D. Jonah, D. Macrillo, R. Tafoya, K. Wesolowski, A. Zulpo, “Low energy accelerator facility upgrade and test,” *Proceedings of 12<sup>th</sup> International Topical Meeting on the Nuclear Application of Accelerators*, Washington, DC, USA, November, 10–13, **2015**.
- [18] J.W. Fowler and F.H. Attix, Chapter 13 in *Radiation Dosimetry*, 2nd edition (eds. F.H. Attix, W.C. Roesch and E. Tochilin) Academic, New York, Vol 2, **1966**.
- [19] C.G. Orton in *Manual on Radiation Dosimetry* (eds. N.W. Holm and R.J. Berry), Dekker, New York, **1970**, p 357.
- [20] J.H. Barrett, *Int. J. Appl. Radiat. Isotopes* 33, 1177, **1982**.
- [21] M. Ragheb, “Radioisotopes Power Production” Nuclear, Plasma and Radiation Science Web text, <http://mragheb.com/NPRE%20402%20ME%20405%20Nuclear%20Power%20Engineering/Radioisotopes%20Power%20Production.pdf>, **2013** (accessed September 2016).







**Nuclear Engineering Division**

Argonne National Laboratory  
9700 South Cass Avenue, Bldg. 208  
Argonne, IL 60439-4854

[www.anl.gov](http://www.anl.gov)



Argonne National Laboratory is a U.S. Department of Energy  
laboratory managed by UChicago Argonne, LLC